



Minnesota State University, Mankato  
Cornerstone: A Collection of Scholarly  
and Creative Works for Minnesota  
State University, Mankato

---

All Graduate Theses, Dissertations, and Other  
Capstone Projects

Graduate Theses, Dissertations, and Other  
Capstone Projects

---

2022

## A Soft-Switched Three-Port DC-DC Converter for a PV/ Battery System

Mohamedelfatih Dosa  
*Minnesota State University, Mankato*

Follow this and additional works at: <https://cornerstone.lib.mnsu.edu/etds>



Part of the [Electrical and Electronics Commons](#), and the [Power and Energy Commons](#)

---

### Recommended Citation

Dosa, M. (2022). A soft-switched three-port DC-DC converter for a PV/ battery system [Master's thesis, Minnesota State University, Mankato]. Cornerstone: A Collection of Scholarly and Creative Works for Minnesota State University, Mankato. <https://cornerstone.lib.mnsu.edu/etds/1263>

This Thesis is brought to you for free and open access by the Graduate Theses, Dissertations, and Other Capstone Projects at Cornerstone: A Collection of Scholarly and Creative Works for Minnesota State University, Mankato. It has been accepted for inclusion in All Graduate Theses, Dissertations, and Other Capstone Projects by an authorized administrator of Cornerstone: A Collection of Scholarly and Creative Works for Minnesota State University, Mankato.

A SOFT-SWITCHED THREE-PORT DC-DC CONVERTER FOR

A PV/ BATTERY SYSTEM

By

Mohamedelfatih Dosa

A Thesis Submitted to the

Graduate College Faculty at Minnesota State University, Mankato

In Partial Fulfillment of the Master of Science Degree Requirements

In

Electrical Engineering

Under the Supervision of Professor Jianwu Zeng

Mankato, Minnesota

November 2022

November 3rd, 2022

A soft-switched three-port DC-DC converter for a PV/Battery System

Mohamedelfatih Dosa

This thesis has been examined and approved by the following members of the student's committee.

---

Jianwu Zeng  
Advisor

---

Vincent Winstead  
Committee Member

---

Huang Han-Way  
Committee Member

## ABSTRACT

This thesis proposed a soft-switched three-port bidirectional DC-DC converter for managing the power flow of a photovoltaic (PV) and battery system.

The proposed converter consists of three ports connected to a PV panel, battery, and load. These three ports are interfaced through the high-frequency transformer and use phase-shift control to achieve soft-switching for all converter switches.

Compared with the traditional multiport converters, the proposed three-port converter uses the least number of power switches, and zero-voltage switching (ZVS). Simulation and experimental results validate the design and effectiveness of soft switching and power flow control. The converter can work in different scenarios regardless of the availability of renewable energy and the battery's state of charge.

In addition, maximum power point tracking (MPPT) for renewable energy sources can be achieved for the renewable energy source while managing the power flow between three ports.

## ACKNOWLEDGMENT

First, it gives me great pleasure to express my heartfelt appreciation and gratitude to Dr. Jianwu Zeng, my academic advisor, who has always helped me understand the fundamental concepts of power electronic engineering and Simulink simulation, his office and lab doors were always open to me, even on the weekends, whenever I had questions about my research or successfully completing my thesis.

His dedication, genuine interest, and, above all, his overwhelming desire to assist his students were primarily responsible for the completion of this thesis and many of my fellow colleague's theses that he was advising. I would say it would be impossible to go through this journey without his support.

Then, I'd like to thank my committee members, Dr. Huang Han-Way and Dr. Vincent Winstead, for their time and effort in becoming members of my committee, as well as their constructive criticism and advice.

Also, I would like to thank everyone at Minnesota State University-Mankato for their assistance during my studies, especially the professors in the Elec. & Comp. Engineering & Technology department, especially Dr. Zhang, Vincent, who has given me numerous amazing pieces of advice and helped me whenever I needed it.

Finally, I must express my heartfelt gratitude to all my family my son, wife, brothers, sisters, and of course, parents (Abdelrahman Dosa and **Fatima Dossa**) for their daily support.

Special thanks to my mom, who is an important figure in my life, Mom thank you for your love, unwavering emotional and financial support, and constant encouragement throughout my life, my mom is the only reason I could keep going forward.

## TABLE OF CONTENTS

Chapter 1 : Introduction and Background.....	1
1.1 Background.....	1
1.2 Renewable Energy Conversion System.....	1
1.2.1 PV System.....	1
1.2.2 Wind System.....	3
1.2.3 Hydropower Capacity System:.....	4
1.2.4 Energy Storage Systems.....	5
1.3 Micro-grid with RESs and ESSs.....	6
1.4 Outline of Thesis and Objectives.....	8
Chapter 2 : Review of Three port Converters and Related Works.....	9
2.1 Topological Structure of TPCS.....	9
2.2 The Operating Principles of the TPC.....	10
2.3 Analysis and Comparison of the Reported TPC.....	13
2.3.1 Non-isolated TPC.....	13
2.3.2 Partially Isolated TPC.....	16
2.3.3 Fully Isolated TPC.....	19
2.4 Summary.....	22
Chapter 3 : The Proposed TPC.....	24
3.1 The Proposal Topology.....	24

3.2 Operational principle.....	25
3.3 Design Considerations .....	33
3.3.1 ZVS analysis .....	33
3.3.2 Delta Calculation.....	34
3.3.3 Maximum Power Point Tracking of PV System.....	35
Chapter 4 Simulation and Experimental Validations.....	38
4.1 Simulation .....	38
4.2 Laboratory Setup.....	40
4.3 Transformer Design and Calculation of Leakage Inductance .....	41
4.4 Experiment Results .....	44
Chapter 5 Conclusion, Recommendation for future work .....	51
5.1 Conclusion .....	51
5.2 Recommendations for Future Work.....	52
References .....	53

# **Chapter 1 : Introduction and Background**

## **1.1 Background**

Natural energy sources such as petroleum, coal, natural gas, and nuclear, chemical reactions are decreasing daily worldwide at varying rates. After they have been employed extensively in various industries, including power generation and transportation, throughout the past several decades, those natural energy sources will run out sooner than expected, plus the environmental damages they created. Because of these two reasons, a couple of decades ago, the world started investing more and more in clean and sustainable energy sources such as solar and wind, plus those already existing, like hydro and biomass energy. The US Energy Information Administration (EIA) forecasts energy renewable resources contribution in electrical Power grid systems will continue increasing every year, especially non-hydroelectric renewable resources like solar and wind, to be the fastest-growing source of US electricity generation in years to come.

Distributed renewable energy sources will soon likely play a more significant role globally in the electric grid system. Clean energy sources or renewable energy in 2020 contributed 20% of the U.S. electricity generation and are growing fast compared to the other energy resources in the last decade, table1 shows the growth of RES in the previous decade.

## **1.2 Renewable Energy Conversion System**

### **1.2.1 PV System**

A photovoltaic (PV) system comprises one or more solar panels, an inverter, and other electrical and mechanical components that convert solar energy into electricity. PV systems come in various



sizes, ranging from small top-roof portable systems to massive utility-scale generation plants [1].

Although PV systems can operate independently as an off-grid or Stand-Alone, often PV System is made up of several individual photovoltaic modules (or panels), usually of 12 volts with power outputs between 50 and 100+ watts each. These PV modules are combined into a single array to give the desired power output.

### **1.2.1.1 PV Work Principle and Main Components**

The PV effect occurs when light from the Sun, composed of packets of energy called photons, falls onto a solar panel and generates an electric current. Each panel generates a fraction of energy but can be connected to other panels to generate more significant amounts of energy, for high-power applications or grid-tied conditions, the output power and voltage are generated by a group series and parallel combinations of PV cells (solar array).

The electricity generated by a solar panel (or array) is direct current (DC). Although many electronic devices, such as cell phones, laptops, and Hybrid and electric vehicles, use direct current electricity, they are designed to operate on the electrical utility grid, which delivers alternating current (AC). As a result, before solar electricity can be injected into the grid for use, it should be converted from DC to AC using an inverter and injected into the grid.

PV system has simple components such as a solar panel comprising several solar cells with semiconducting properties. And an inverter is a type of electrical device that receives direct current (DC) and transforms that into alternating current (AC). Racking refers to the structural system that secures the solar array to the floor rooftop [1].

$$E = h \cdot c / \lambda \quad (1.1)$$

where  $E$  is the energy absorbed in electron-volt (eV),  $h$  is planks constant ( $6.62 \times 10^{-27}$  erg/s),  $c$  is light speed ( $3 \times 10^8$  m/s), and  $\lambda$  is the wavelength of light radiations.

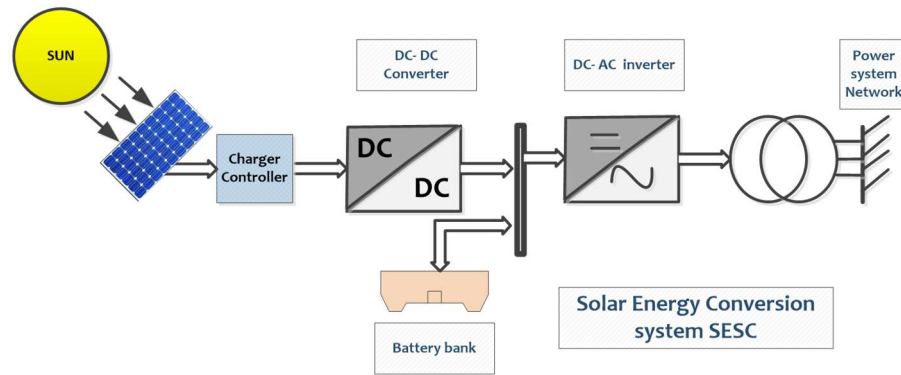


Figure 1.1 Solar energy conversion system interfacing with Grid

### 1.2.2 Wind System

Wind energy conversion systems (WECS) convert wind energy into mechanical energy. Then Wind turbine generators convert mechanical energy to electricity, and the Generated power is employed in various fields, industrial, commercial, or residential [2].

The progress of WECS has been remarkable over the past several years. Turbines, machinery, drives, and protective devices have all undergone significant improvements because of the development of new technology [2]. Many different generators are available to power a wind turbine, including an induction generator, a double-fed induction generator, a permanent magnet synchronous (PMSG), etc.

The generator receives the power generated by the wind turbine. Then the pulse width modulation converter is used to control the generator's rotational speed to get the maximum output power of the WECS, the generator-side converter. A grid-side inverter supplies the generator's output power to the grid.

Wind energy conversion systems and solar energy conversion systems are becoming the most promising and reliable renewable energy in the future, due to many merits such as being environment-friendly, sustainable, and low running cost...etc., one option for distributing wind farms is to use them in flat or hilly terrain.

Also, the WCES is one of the most promising power sources in the future. The kinetic energy of wind captured by a turbine's blades per unit time ( $P_{out}$ ) is proportional to the density of the air ( $\rho$ ), the area swept by the rotor blades ( $\pi r^2$ ), and the cube of the wind speed ( $v_{wind}^3$ ) multiplied by an efficiency or power factor ( $C_p$ ) as showing in equation 1.2.

$$P = \frac{1}{2} \cdot \rho \cdot \pi \cdot r^2 \cdot C_p(\lambda, \beta) \cdot v_{wind}^3 \quad (1.2)$$

Figure 1.2 below shows the WECS interconnection to the power system grid.

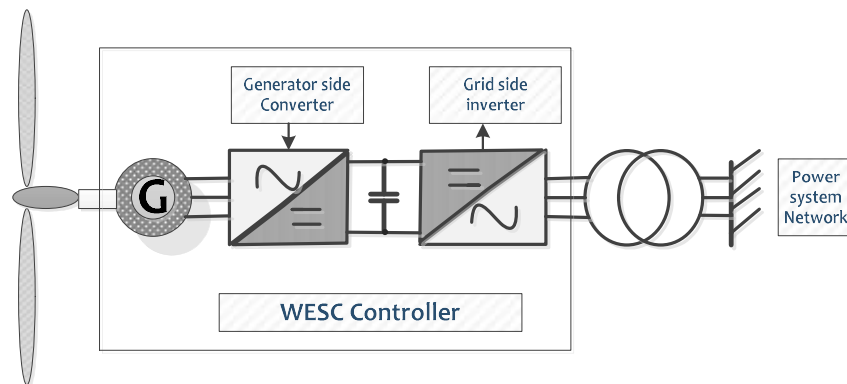


Figure 1.2 Wind energy conversion system interfacing with Grid

### 1.2.3 Hydropower Capacity System:

The second most contributed source of clean energy in the United States last year was of US energy information Administration (EIA), since hydroelectric electricity is generated by water, hydroelectric power stations are often built on or near a body of water. The volume of water flowing and the change in elevation influence the amount of electricity produced in flowing water

Generally the more significant the water flow or, the greater height, the more energy can be generated by a hydroelectric plant [3].

Hydroelectricity's percentage of overall electricity production in the United States has dropped over in recent times, primarily because of its impact on nature and biodiversity.

However, several hydroelectric power plants are incorporating with solar energy as an extended form of resource. There are mainly three types of hydroelectric power plants impoundment, diversion, and pumped storage [4].

#### **1.2.4 Energy Storage Systems**

The growing demand for electric energy for residential to commercial, as well as the newly growing electric vehicle (EVs) industry, made it crucial to have the ability to store the energy. Since we have a continuous demand for electricity and some of the modern RES fluctuates depending on the weather or can only be generated electric power when the sun is shining, the need for electricity storage has increased rapidly [5]. Due to this reason, energy conversion and energy storage have drawn much interest from different energy consumption sectors. Energy Storage Systems (ESSs) are highlighted as a critical solution for mitigating the intermittent nature of RESs and providing the load or grid with an uninterruptible power supply (UPS) [6] [7].

Batteries are commonly used for storing electrical energy, ranging in size from the button cells used in watches to megawatt load leveling applications. Batteries can be divided into two classifications: electrochemical batteries and fuel cells. Fuel cells that utilize liquid fuels like methanol are referred to as primary batteries because they are typically not rechargeable and need to be recharged before they run out, making them unsuitable for repeatedly storing energy.

Electrochemical batteries, such as Lead–Acid and Li-oxygen batteries, can have high energy storage, but their output power is limited.

### 1.3 Micro-grid with RESs and ESSs

Micro-grids may be a future power system that solves the renewable energy technologies (RET) that are required to support the increasing deployment of distributed energy resources (DER), mainly small-scale combined heat and power (CHP) and small-scale RES.

The micro-grid system is a smaller scale of the smart grid. It is generally considered a single controlled entity, co of a central controller unit and a group of localized electrical consumers (or users) associated with RESs and energy storages plus transmission lines and other facilities as shown in Figure 1.3 [8].

Numerous installations throughout the globe are doing active experiments in the micro-grid domain are presented, and the primary benefits of micro-grids focus on three aspects flexibility of the power system, the possibility to adjust the quality of power given to end users, and a more favorable environment small-scale renewable generation investments [9] [10].

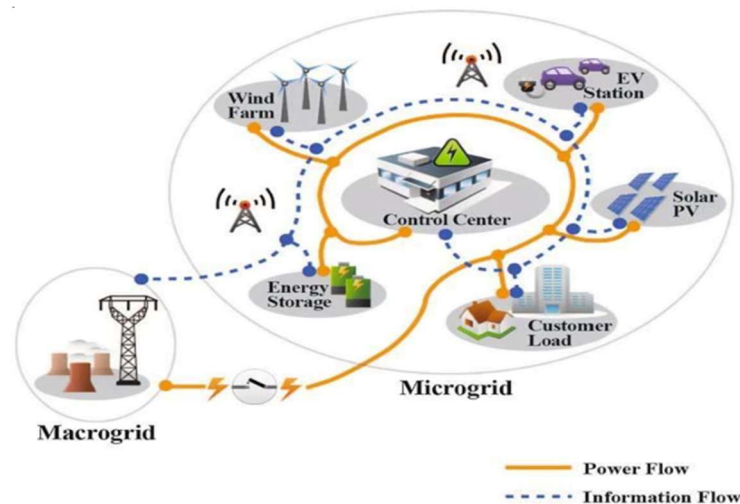


Figure 1.3 Typical Macro-grid schematic [8].







Micro-grids have other advantages, such as they can work in isolated mode and grid connected mode. A grid-connected mode is the one that the local utility grid (Micro-grid) is connected to the main grid at a point of common coupling that maintains voltage at the same level as the main grid, so that when RESs produce more electricity than the load, the surplus power is fed into the grid.

It will remain on the grid unless there are some problems or maintenance need to be performed on the grid or other reasons to be disconnected. A switch can connect or disconnect the microgrid to (or from) the main grid automatically or manually.

An island mode is not connected to the main grid, the local sources undertake the job of catering to the loads.

Table I shows how much renewable energy has increased in the last decade [11].

Table I: Increment of the electrical power source in the last decade

No.	Type of power	Billion KW/H		% Increment in the last Decade
		2010	2020	
	Hydropower Capacity	260.20	291.11	12%
	Solar PV Capacity	1.21	90.89	7412%
	Wind power capacity	94.65	337.51	257%
	Biomass power Capacity	56.09	56.05	0%
	Geothermal Power Capacity	12.22	16.94	39%
	<b>Total</b>	<b>424.37</b>	<b>792.50</b>	<b>87%</b>

## 1.4 Outline of Thesis and Objectives

Following the above introductions in chapter one, an outline of this thesis is given as follows.

Chapter 2: Review of Three port DC-DC converters and related prior works, discussing more about the topologies Derivation and modeling techniques ending the chapter by summarizing.

Chapter 3: The proposes DC-DC three-port converters for solar, and battery systems. The topology, operating principles, ZVS analysis, MPPT, and the power management control strategy and discussing the differences from the existing ones.

Chapter 4: Simulation result, Experimental work describes the prototype used in the experimental setup to validate the simulation to achieve the design objective; a method of maximum power point tracking (MPPT) is developed to explain the operational optimization of the power source (solar energy).

Chapter 5: Finally, this Thesis ends with conclusions, a summary of contributions, and recommendations for future work.

## Chapter 2 : Review of Three port Converters and Related Works

### 2.1 Topological Structure of TPCS

Traditionally, the renewable energy source is connected to the power system load or the micro-grid via a traditional DC-DC converter. The energy storage system is connected to the input port or output port of the conventional DC-DC converter via a bidirectional DC-DC converter for charging and discharging the ESS, as illustrated in Figures (a) and (b) below.

The core problem of these methods is their poor efficiency, as they need an extra converter for the ESS. Furthermore, the multi-stage design may lead to bulk hardware, poor power density, and relatively of excessive cost [12].

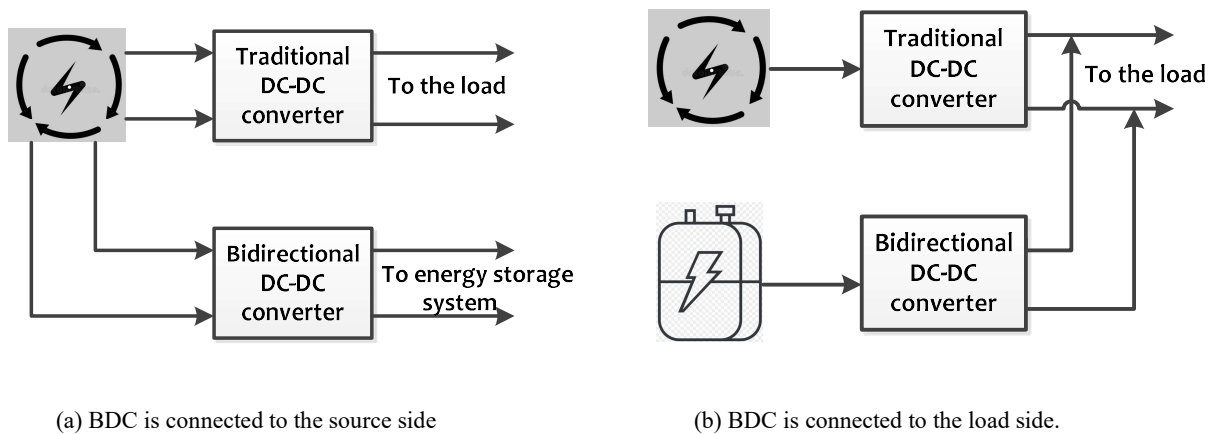


Figure 2.1 The traditional power electronics in RECS

In recent years, many TPC with typical structures, as shown in Figure 2.2 below, have been developed to integrate renewable energy sources and energy storage converters into a single converter that has two inputs: one is for the PV panel, and the other is for charging and discharging the ESS.



The third port is the output port of the TPC, which might be directly linked to a DC load or the micro-grid through an inverter via a DC link capacitor. Numerous TPCs that are capable of MPPT and energy-storage charging and discharging.

In general, the TPC can be classified into three categories according to their coupling structure & galvanic isolation requirements, non-isolated topologies [16]-[23], partially isolated topologies [26]-[33], and fully isolated topologies [38]-[44].

## 2.2 The Operating Principles of the TPC

Figure 2.2 illustrates the overall structure of a renewable energy generating system using a TPC. The general structure figure shows that the input ports are connected to the RES and battery, and the output port is connected to the load.

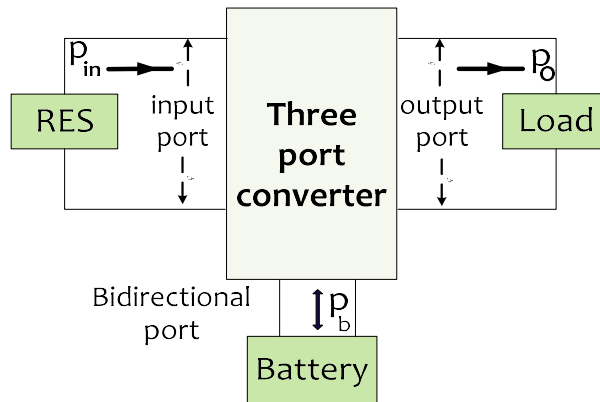


Figure 2.2 The general structure of the TPC.

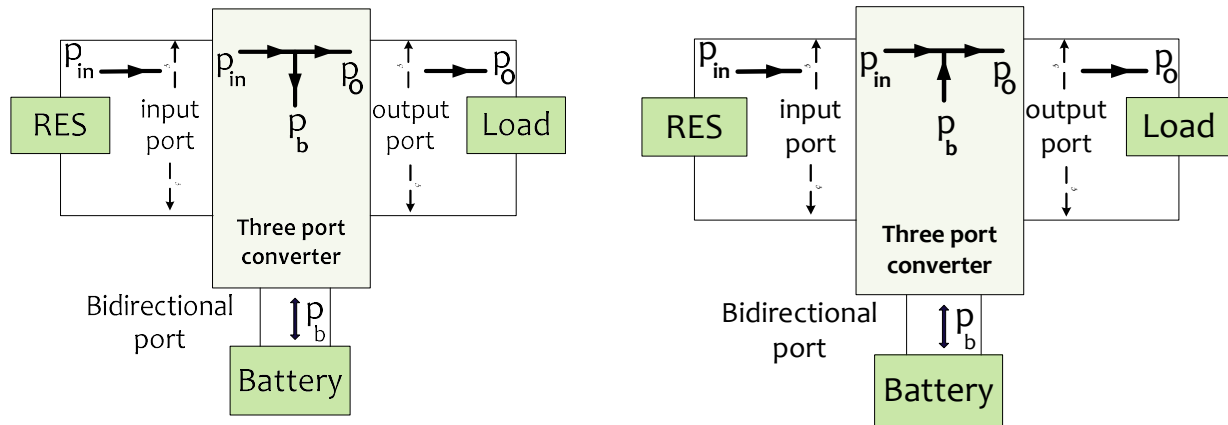
Within the framework of the power-balance concept, the relationship between the three ports' powers may be represented as follows:

$$P_{in} = P_b + P_o \quad (2.1)$$

where  $P_{in}$  denotes the input power;  $P_b$  is the battery power, and  $P_o$  is the output power. The TPC mainly has three operation modes which are basically depending on the source's availability and the grid demand and can be categorized as follows.

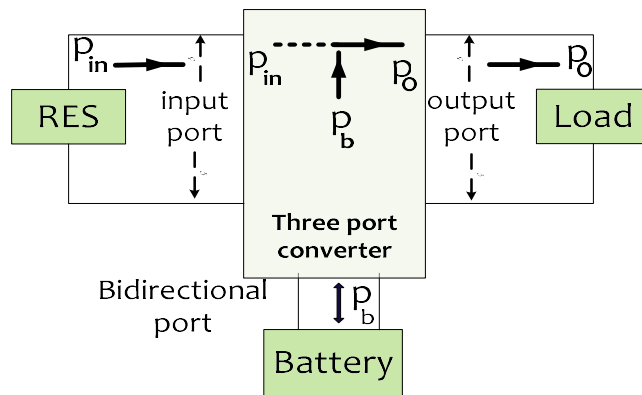
1. Single input dual output mode (illustrated in Figure 2.3 (a)): this is when the source of the power (Photovoltaic panel) produces more power than the load needs ( $P_{Pv} > P_{Ld}$ ), then the extra energy will be used to charge the batteries ( $P_{Pv}-P_{Ld}$ ), and in this case, the battery power will be more than zero  $P_B > 0$ ,  $P_{Pv} = P_B + P_{Ld}$ .
2. Dual input single output mode (illustrated in Figure 2.3 (b)): this mode occurs when the solar power is not sufficient to satisfy the load demand ( $P_{Pv} < P_{Ld}$ ), then the battery discharge power to compensate the shortages of the power,  $P_{Ld} = P_B + P_{Pv}$ .
3. Single input single output mode (illustrated in Figure 2.3(c)): the solar power zero ( $P_{Pv} = 0$ ) the battery alone provides power to the load.

According to converters' control principles, N-1 independent control variables are required for an N-port converter [13], however, TPCS requires two independent control variables. Typically, one control variable must strictly and independently regulate the output port's voltage, while the other control variable must regulate either the PV or battery port's voltage. Notably, one of the PV ports and one of the battery ports must remain flexible to achieve power balance at any period. To summarize, TPCS requires at least "three power transmission branches and two independent control variables, it is evident that different power transmission branches are necessary for TPCS for different operation modes [13] [14].



(a) Single input dual output mode

(b) Dual input single output mode



(c) Single input single output mode

Figure 2.3 The general architecture of three port converter operating modes

Based on the three mods above and the control principles of the TPCs, there are two convenient paths for the power to be transmitted to the load, one is directly from the PV panel port to the load (P2L), also called primary power transmission path, and the other is from or through the battery to the load (B2L) also called secondary power transmission path, the arrays in Figure 2.3 shows power transmission diagram paths. Each branch's power transmission may be accomplished using

a unidirectional two-port dc–dc converter that requires a minimum of one independent control variable like duty cycle, frequency, phase, and so on [15].

## 2.3 Analysis and Comparison of the Reported TPC

### 2.3.1 Non-isolated TPC

Non-isolated three-port converters have advantages and disadvantages, those types of converters can reduce the number of elements and have a much more compact design. That can be an advantage and disadvantage due to the direct connection of the converter element, it is only suitable for applications that do not require galvanic insulation [16], and also, those types of converters have limitations on the voltage gain, and that because the voltage conversion ratio's modulation flexibility is limited to the duty cycle. To address these issues, some proposed utilizing coupling inductor technology to increase the voltage conversion ratio [17], Figure 2.4 illuminates the three-port conversation.

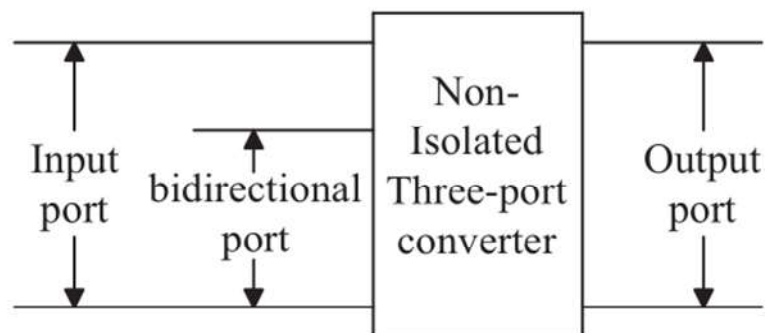


Figure 2.4 The general configuration of non-isolated TPC

Numerous non-isolated three-port DC-DC converters with various control and modulation approaches have been published in the last few years. The conductor is the critical element in the

TPC, some of the proposed TPC uses a single inductor to increase the power density and decrease the TPC size, and while on the other hand, some utilize two or more inductors.

Because most of these converters are based on standard boost, buck, and buck-boost converters, their gain is limited. Several three-port DC–DC converters use linked inductors to increase the voltage conversion ratio to overcome this limitation.

Figure 2.5 shows a typical non-isolated converter with a single inductor, that is proposed for PV and battery applications [16] [18], the proposed converters are derived from a dual-input converter by adding a new power flow path, which means adding a new control variable, different control techniques are used here to control the power flow between any two of the three ports [16].

*Figure 2.6* shows a novel non-isolated TPC proposed in [19], the proposed converter mixes a typical boost converter and a buck converter with an additional switch to control the output power.

Figure 2.7 shows the proposed three port converter that combines an electronic circuit, which consists of a diode, a switch, and an energy storage system in parallel with the inductor, into a typical buck-boost converter, a two-switch single-inductor three-port converter proposed in [20], and examined in [21]. Additionally, this general cell can be classified into various conventional converters such as buck and boost converters, to develop new three-port converters, more details in [20].

Figure 2.8 shows A three-port converter with three switches and three inductors is proposed in [22] by combining a two-inductor boost converter and a two-inductor buck converter and utilizing an extra inductor to achieve the voltage-second balance to all inductors.

Figure 2.9 shows a three-port DC-DC converter with a high voltage conversion ratio based on a unidirectional three-state switching cell that has been proposed in [23], the proposed converter structure has natural properties that make all the converter switches operate under soft-switching

conditions throughout an extensive operating range and that decreased voltage stresses, resulting in an excellent overall efficiency this converter has many advantages not limited to such as high gain, high efficiency, and soft switching, all that were validated in the laboratory by a 500W prototype, more detail in [23].

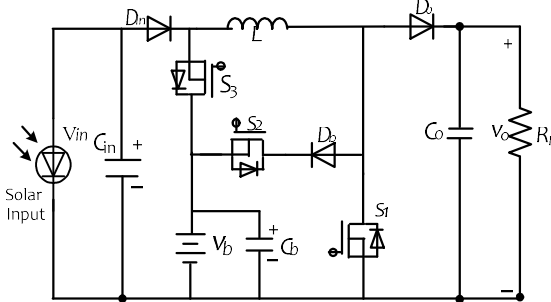


Figure 2.5 The proposed converter in [18].

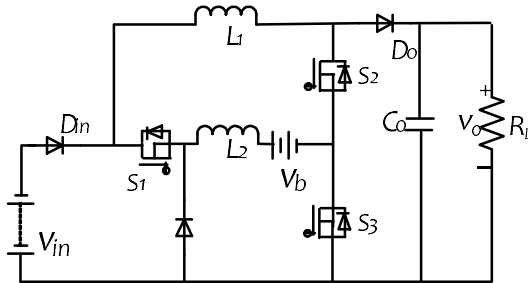


Figure 2.6 The proposed converter in [19].

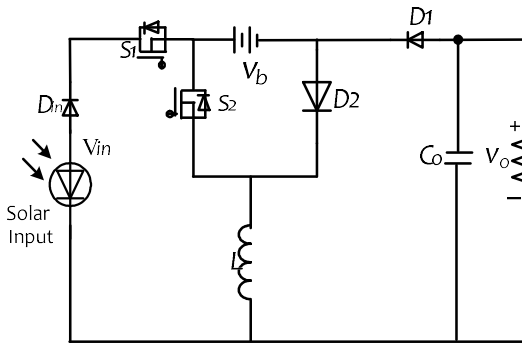


Figure 2.7 The proposed converter in [20].

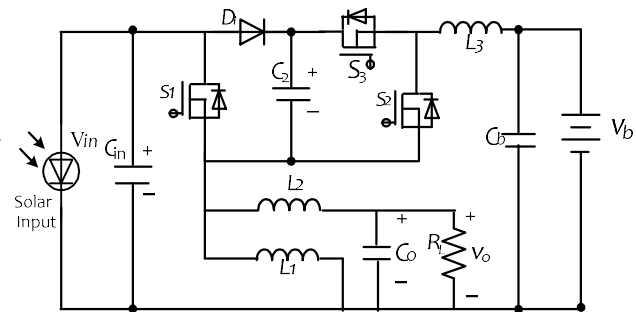


Figure 2.8 The proposed converter in [22].

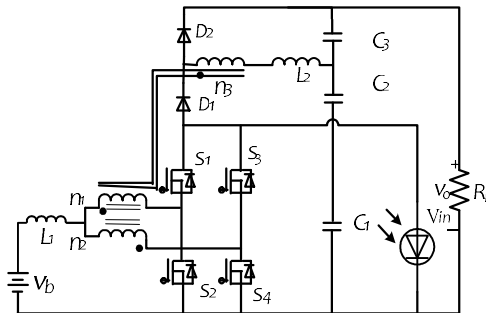


Figure 2.9 The proposed converter in [23].

### 2.3.2 Partially Isolated TPC

Partly- isolated three-port converters, that use a high-frequency transformer to isolate one port from the other two ports, there are two connecting methods of the partially isolated converters depending on the isolated port, the source port or the load port, most of these types of converters usually have the source port and the bidirectional port connected directly, and then they are connected to the isolated load port through the transformer, while the other connected the bidirectional port with the load port then connect the combination through the high-frequency transformer to the source port Figure 2.10 illuminate the TPC configuration. In this type of converters, the high voltage gain can be obtained by a large turn ratio, these converters operating modes are DIDO or SISO, which make the energy storage system under continuous operation resulting in shortened life of the energy system as well as make the overall system less reliable, below are some of the partly- isolated three-port converters.

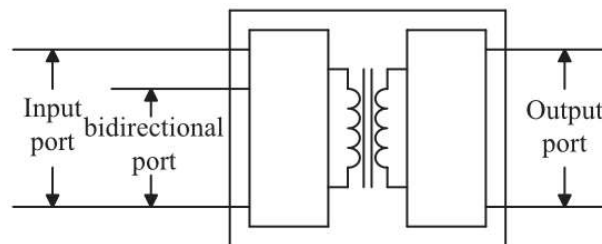


Figure 2.10 The general configuration of a partially isolated three-port converter

Figure 2.11 shows a three-port DC–DC converter based on the half-bridge converter proposed and analyzed in [24] and [25]. The proposed converter is derived from the traditional half-bridge converter by applying an additional switch and a diode on the primary side of the transformer and using two switches to replace the diode in the output port.

All the switches on the primary side can operate under zero voltage switching for a wide range of operation conditions. Controlling the power flow between the three ports is accomplished by adjusting the duty cycles of the two primary side switches.

Figure 2.12 also shows a buck-boost three-port DC–DC converter with a full-bridge switching cell, proposed in [26]. In the proposed converter, the primary side of the transformer is constructed in a way that makes it more compact to help eliminate the ripple current. At the same time, the secondary side uses a half-bridge switching cell.

Also, the proposed TPC used phase shift with pulse width modulation technique as a simple way to distribute power among the converter ports. More details can be found in [26].

Figure 2.13 shows a proposed partly-isolated three-port DC–DC converter for a stand-alone renewable power system application derived from the half-bridge converter in [27].

The bidirectional port consists of two input dividing capacitors plus the storage system and shares two switches with the input port to allow the biased DC current in the transformer to cause the power to flow between the input port and the bidirectional port. All ports' voltage is regulated through independent controllers and the two switches on the secondary side for synchronous regulation.

A similar converter configuration has been reported in [28] with some modifications by adding post-regulation to replace the synchronous regulation in the converter. All the obtained converters have the advantages of a reduced number of components and relatively simple configurations. The efficiency of these converters is relatively high as the power flow between any two of the three ports is in a single stage.

Figure 2.14 shows a proposed converter different from the previous converters; in all the above examples, the integrated ports are the input and bidirectional ports in the primary side of a high-



frequency transformer, isolated at the secondary side of the transformer. In this proposed novel partly isolated converter, the integrated ports are the bidirectional port, and the load is to the secondary side of the high-frequency transformer. The PV is isolated at the primary side of the high-frequency transformer.

The detailed derivation of the proposed converter from the traditional half-bridge converter is introduced in [29]. The output circuit of the traditional half-bridge converter is detached first, and then a boost converter is inserted between the two detached outputs to provide the power flow path between the battery and the load. In the input port, a boost converter is applied to help reduce the ripples of the input current. All the switches in this converter can work under zero current switching conditions to reduce the switching losses and improve the converter's overall efficiency.

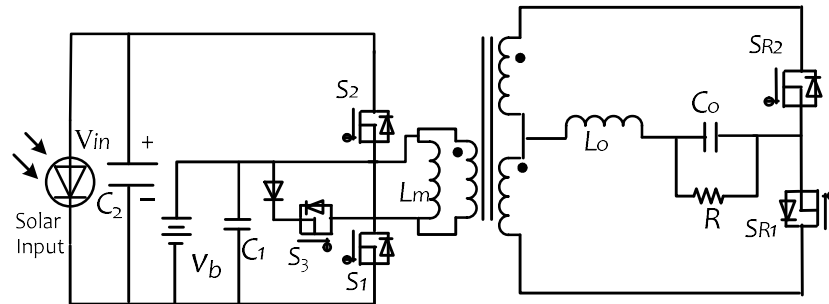


Figure 2.11 The proposed converter in [24].

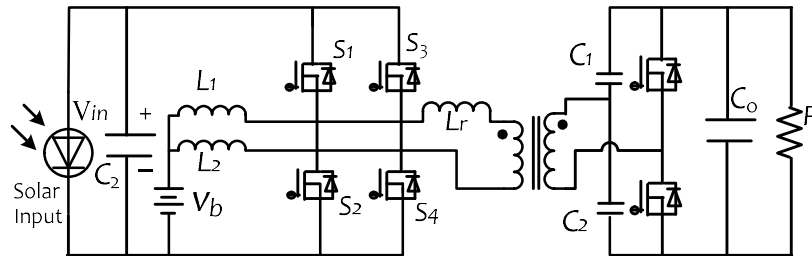


Figure 2.12 The proposed converter in [26].

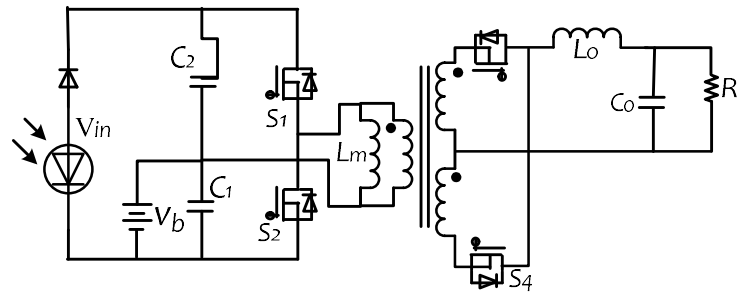


Figure 2.13 The proposed converter in [28].

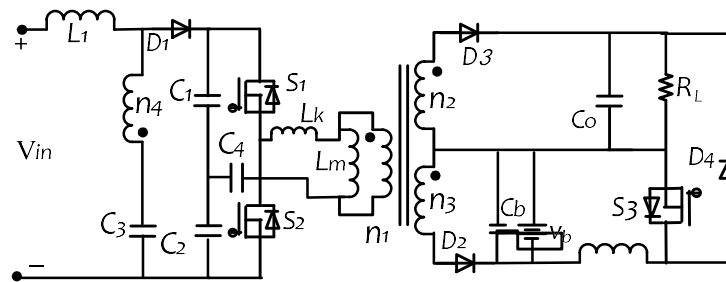


Figure 2.14 The proposed converter in [29].

### 2.3.3 Fully Isolated TPC

Fully isolated three-port DC-DC converters have completed good galvanic isolation because the power flows from one port to another through a multiple-winding high-frequency transformer. So, any port has its components, and most fully isolated converters use full-bridge or half-bridge converters and, in some cases mix of both. Usually, the structure of this type consists of a combination of a three full-bridge structure and a three-winding model that includes two additional series resonant circuits in the primary side of the transformer, to implement the soft switching of the switches to reduce the switching losses. One of the advantages of this converter from the non-isolated and the partially isolated is that it can switch at a high frequency while maintaining realizable element values. Figure 2.15 shows this type of isolated TPC configuration.

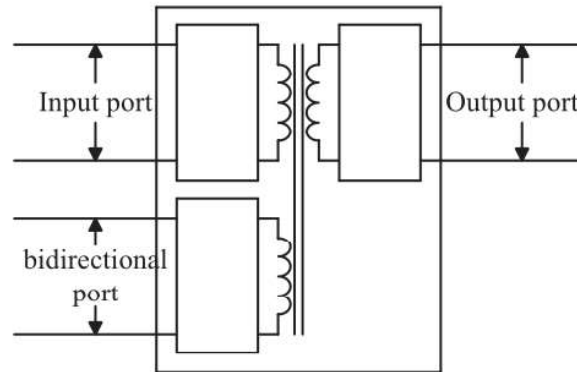


Figure 2.15 The general configuration of the bidirectional, DC-DC converter

Figure 2.16 shows the first fully isolated DC-Dc three-port converter was proposed at [30], the proposed converter consists of a combination of a three full-bridge structure and a three-winding, even though it was designed for use in hybrid fuel cell systems, it may also develop to be applied in other renewable energy applications such as photovoltaic production systems. Following the release of this converter, it attracted considerable interest from other researchers in developing and studying the converter performance, analyzing the control methods, loss analyses, and applications that will be using the converter. Then later on and to increase the efficiency converter's efficiency and minimize the input current's ripples, the proposed converter came after that, suggesting adding an inductor between the input source and the full-bridge structure in the input port [30].

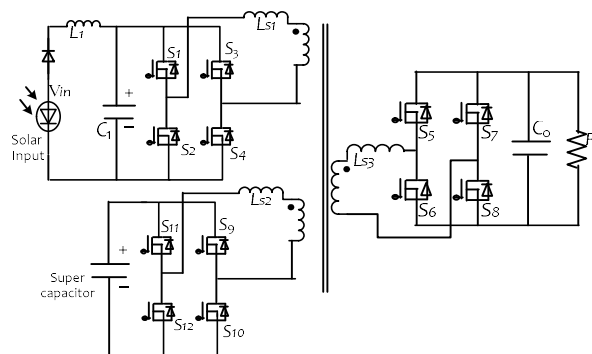


Figure 2.16 The proposed converter in [30].

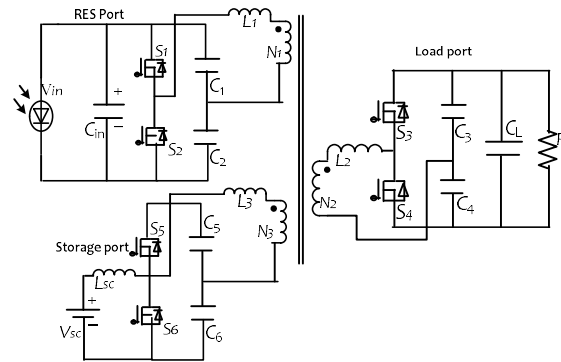


Figure 2.17 The proposed converter in [31].

Figure 2.17 above shows the proposed novel three-port DC converter presented in [31] by substituting the full-bridge structures in the converter with three half-bridge structures. It is to be observed that this converter has three half-bridge circuits, one of which is a boost half-bridge converter that connects to the bidirectional port for the energy storage system's charging and discharging functions. The converter shows much improvement when working in single input double output mode.

A novel isolated three-port DC-DC converter is presented in as [32] shown in Figure 2.18. It is based on employing two current fed switching networks and two multi-resonant circuits as the input port and the bidirectional port, respectively, with a high-frequency transformer and using a full-bridge diode rectifier as the output port.

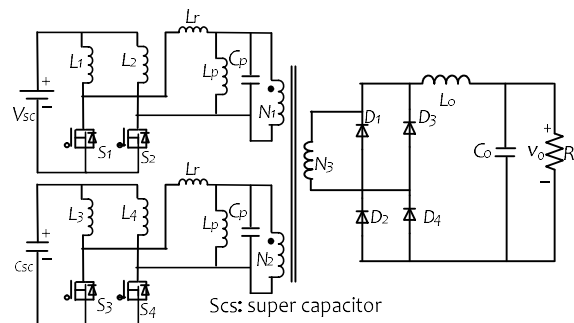


Figure 2.18 The proposed converter in [32].

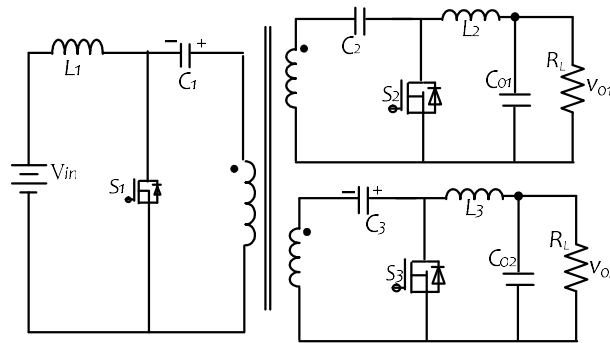


Figure 2.19 The proposed converter in [33].

This converter is less expensive because it needs four switches instead of the more expensive, isolated converters mentioned above. Due to the use of inductors in all three ports, the converter's current ripples are also relatively low. Converters of different configurations can also be utilized to create three-port converters in addition to the half-bridge and full-bridge versions. Based on the conventional Cuk converter, a novel isolated three-port DC-DC converter with only three switches has been disclosed in [34]. As a fully isolated converter, it applies a three-winding transformer, as illustrated in Figure 2.19, to incorporate three Cuk converters.

## 2.4 Summary

This chapter provided an overview of novel topologies of three-port DC-DC converters that proposed to discuss how to benefit from using renewable sources for energy storage by using only one converter with two input sources and one output instead of the separate three converters. Several previous proposed TPC converters were reviewed by discussing their derivation and modulation techniques. The three-port DC-DC converters proposed during the past ten years are numerous, but depending on the application, construction, reliability, performance, cost of the control circuits, number of components, etc., they all have various advantages and disadvantages.

Typically using a smaller number of power switching devices that minimizes the number of components in the Non-isolated TPC circuit, as well as the requirement to use a high-frequency transformer for isolated and partially isolated converters, the structure of the non-isolated can usually result in a lower cost than the partially isolated and isolated converters.

Reliability is an important aspect to consider when assessing converters' performance. For all converters, dependability will decline throughout the operation time under consideration. The reliability of the converter decreases with the number of switches it uses at the module. As the cost, the more switches a converter utilizes at a module, the less reliable the converter becomes. All the three-port converters proposed are adept at MPPT control and ZVS and can meet the necessary load demand with an energy storage system, various restrictions can be applied to the converters' use because of their design.

For small power applications, such as portable devices, the non-isolated TPCs are suitable but not suitable for high voltage applications requiring strong galvanic isolation; in these cases, partially isolated and fully isolated TPCs are preferable options.

## Chapter 3 : The Proposed TPC

### 3.1 The Proposal Topology

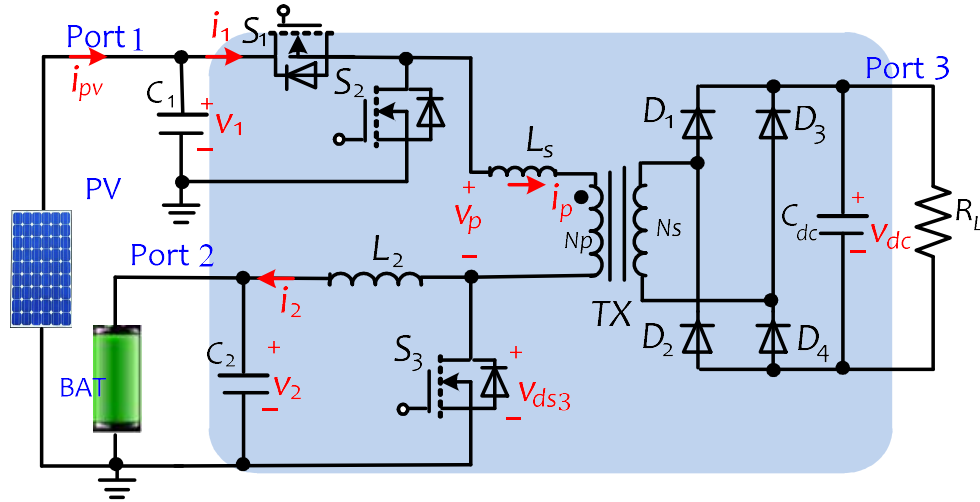


Figure 3.1 Topology of the proposed Three-port DC-DC converter.

The circuit diagram of the proposed three-port DC-Dc converter is shown in Figure 3.1, which is coupled to two different power supplies, Port1 and port2, Port one is contacted to the PV panel, and port two is connected to the Battery bank, and there is a third port which is connected to the load or the grid.

The switches  $S_1$  and  $S_2$  plus the capacitor  $C_1$  are connected in parallel with the PV panel representing the main components of Port1 (the PV panel port), The resonant circuit  $L_2C_2$  is connected in parallel with the Battery bank plus switch  $S_3$  representing port2, in this port the batteries are modeled to be an ideal with internal resistant  $r_b$ .  $V_b$  is the voltage across the battery terminals, and the  $V_o$  is the port open circuit volt, as illustrated in Figure 3.2(a).

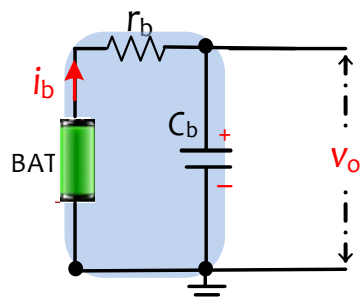


Figure 3.2(a) Battery equivalent circuit

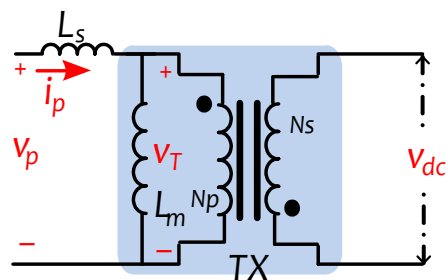


Figure 3.2(b) Transformer equivalent circuit

Figure 3.2 The equivalent circuit for the battery and the transformer.

Those two ports are the input ports, and they are connected to the low-voltage-side (LVS) of the high-frequency transformer, whose turn ratio is described as  $n = N_p / N_s$ , where  $N_p$  and  $N_s$  indicate the primary and secondary winding turns, respectively. According to the definition of transformer ratio  $N_p/N_s$ , the transformer is represented as a magnetic inductor  $L_m$  connected in series with an ideal transformer and parallel with a leak inductor  $L_s$  as illustrated in Figure 3.2(b), the transformer equivalent circuit. And the power Diodes  $D_1$ ,  $D_2$ ,  $D_3$  and  $D_4$  which work as Full-Wave Rectifier connected to  $C_{dc}$  in parallel are the load port's main components.

### 3.2 Operational principle

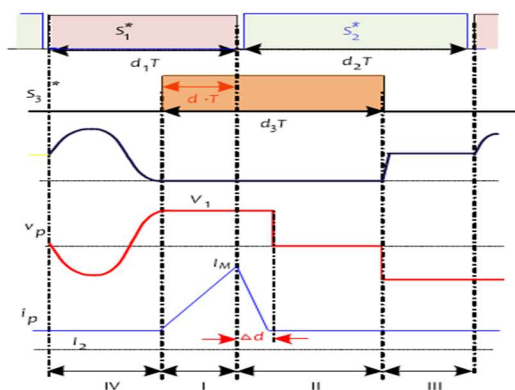


Figure 3.3 The proposed converter operation stages



Figure 3.3 illustrates the gate signals (PWM) of the three switches as well as the voltage  $V_p$  throughout the primary side of the transformer.

When the switch is turned on,  $S_n^*$  equals one otherwise,  $S_n^*$  equals 0, the PWM of the first two switches  $S_1$  and  $S_2$ , are switching in a complementary manner with duty cycles 0.5,  $S_1$  and  $S_2$  complementary duty cycles can be altered from 0 to 1.  $S_3$  also has a duty cycle of 0.5.

The proposed TPC consists of four operating stages, I, II, III and IV, based on the statuses of the three switches and the duty cycle (d) values.

Due to the similarity of analytic methodologies in different operating stages, this study analyzes just one operation stage, namely  $d_1 > 0.5$ ,  $d_2 < 0.5$ , and  $0.5 < \delta < d_1$ , where  $d_1$  and  $d_2$  are the duty cycles of  $S_1$  and  $S_2$ , respectively.

As I mention, the duty cycles of the  $S_1$  and  $S_3$  are 0.5, and the PWM of these two switches is complimentary. The complementary duty cycle of  $S_1$  and  $S_2$  can be changed from 0 to 1. The phase difference of the duty cycles of  $S_1$  and  $S_3$  is defined as absolute  $\delta$ .

The four stages and their equation describing as follow:

$$\begin{cases} L_s \cdot \frac{di_p}{dt} = v_1 - V_T - v_{ds3} \\ L_2 \cdot \frac{di_2}{dt} = v_{ds3} - v_2 \\ C_2 \cdot \frac{dv_2}{dt} = i_2 - \frac{v_2 - v_b}{r_b} \end{cases} \quad (3.1)$$

Stage I:

In this stage,  $S_1$  and  $S_3$  are activated while  $S_2$  is deactivated, a positive voltage is applied to the primary side of the transformer,  $V_P = v_1$ , and the PV energy is sent straight to the load side. This stage will continue to run until switch  $S_1$  is off. The initial current on the primary side of the transformer  $i_p(0)$  is equal to  $I_2$  ( $i_p(0) = I_2$ ), the transformer voltage  $V_T > 0$ , and  $V_{ds3} = 0$ .

The equivalent circuit is shown in Figure 3.4.

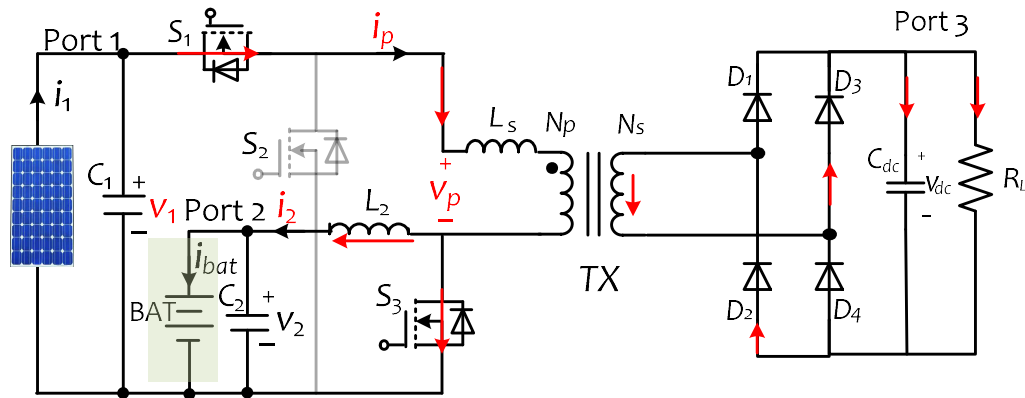


Figure 3.4 The operation states of the proposed converter Stage I

The differential equations of this stage may be represented as follows.

$$L_s \cdot \frac{di_p}{dt} = v_1 - V_T \quad (3.2)$$

$$i_p = I_2 + \frac{V_1 - V_T}{L_s} \cdot t \quad (3.3)$$

Where  $L_s$  is the leakage inductance on the primary side of the transformers and will explain more about it and its calculation later in this chapter, and at the end of the stage:

$$I_M = I_2 + \frac{V_1 - V_T}{L_s} \cdot (d_1 - \delta) \cdot T \quad (3.4)$$

Stage II:

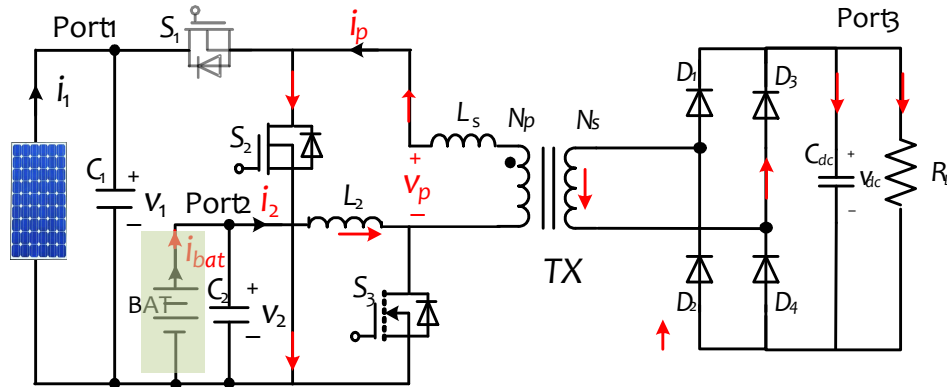


Figure 3.5 The operation states of the proposed converter stage II

This stage started when  $S_1$  turned off, and  $S_2$  turned on while there was no change in the status of  $S_3$ . After  $S_1$  turned off, the PV voltage dropped  $v_1 = 0$  and  $V_{ds3} = 0$ , while  $V_T > 0$ .

Figure 3.5 shows the equivalent sub circuit of the stage, then we can express the stage differential equations as follows.

As follow

$$i_p = I_M - \frac{V_T}{L_s} \cdot t \quad (3.5)$$

When  $i_p$  drops to  $I_2$ , the duration time

$$\Delta d = L_s \cdot \frac{I_M - I_2}{V_T \cdot T} \quad (3.6)$$

$$i_2 = I_2 - \frac{V_b}{L_2} \cdot (\delta + \Delta d) \cdot T \quad (3.7)$$

At the end of this stage,  $S_3$  is turned off, achieving ZVS, the transformer voltage  $V_T = 0$ , and primary current  $i_p = I_2$ .

$$i_p - i_2 \approx \frac{V_b}{L_2} \cdot \delta \cdot T \quad (3.8)$$

Stage III:

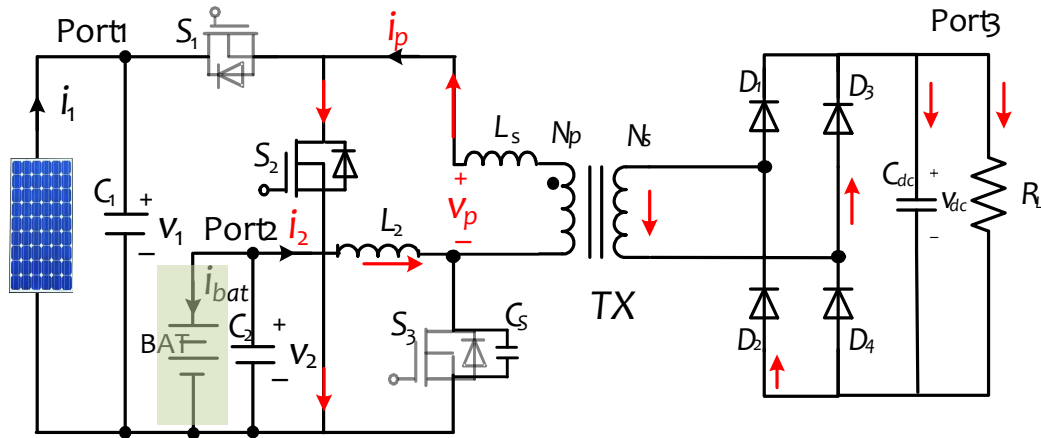


Figure 3.6 The operation states of the proposed converter stage III

In this stage,  $S_3$  is turned off while the rest of the switches stay the same as that in Stage II  $S_1$  is off and  $S_2$  on, and the initial voltage across the  $S_3$  is  $V_{ds3}(0) = 0$ . Figure 3.6 shows the equivalent sub circuit of the stage and the stage differential equations can be expressed as follows

$$\begin{cases} L_s \cdot \frac{di_p}{dt} = 0 - v_{ds3} + V_T \\ L_2 \cdot \frac{di_2}{dt} = v_{ds3} - v_b \\ C_s \cdot \frac{dv_{ds3}}{dt} = i_p - i_2 \end{cases} \quad (3.9)$$

$$\begin{aligned}
C_s \cdot \frac{dv_{ds3}^2}{dt^2} &= \frac{V_T - v_{ds3}}{L_s} - \frac{v_{ds3} - V_b}{L_2} \\
&= -\left(\frac{1}{L_s} + \frac{1}{L_2}\right) \cdot v_{ds3} + \frac{V_T}{L_s} + \frac{V_b}{L_2} \\
&\approx -\frac{1}{L_s} \cdot v_{ds3} + \frac{V_T}{L_s}
\end{aligned} \tag{3.10}$$

$$v_{ds3} = A \cdot \cos(\omega_{s1} \cdot t) + B \cdot \sin(\omega_{s1} \cdot t) + V_T \tag{3.11}$$

$V_{ds3}(0) = V_T$ ,  $I_{ds3}(0)$  is (9)

$$\begin{cases} v_{ds3}(0) = A + V_T = V_T \\ \dot{v}_{ds3}(0) = \omega_{s1} \cdot B = \frac{V_b}{L_2 \cdot C_s} \cdot \delta \cdot T \end{cases} \tag{3.12}$$

When  $V_{ds3} = V_T$ , there is resonance with small magnitude and low frequency

$$\omega_{s1} = \frac{1}{\sqrt{L_s \cdot C_s}} \tag{3.13}$$

$$v_{ds3} = \sqrt{\frac{L_s}{C_s}} \cdot \frac{V_b \cdot \delta}{f \cdot L_2} \cdot \sin(\omega_{s1} \cdot t) + V_T \tag{3.14}$$

$$\begin{aligned}
v_{ds3} &= \sqrt{\frac{L_s \cdot C_s}{L_2 \cdot C_s}} \cdot \frac{2\pi \cdot V_b \cdot \delta}{\omega} \cdot \sin(\omega_{s1} \cdot t) + V_T \\
&= \frac{\omega_{s2}}{\omega_{s1}} \cdot V_b \cdot \delta \cdot T \cdot \sin(\omega_{s1} \cdot t) + V_T
\end{aligned} \tag{3.15}$$

$$\omega_{s2} = \frac{1}{\sqrt{L_2 \cdot C_s}} \tag{3.16}$$

The oscillation magnitude is small such that the current/voltage stage can be treated as a constant value, at the end of the stage:

$$\dot{v}_{ds3} = \omega_{s2} \cdot V_b \cdot \delta \cdot T \cdot \cos[\omega_{s1} \cdot (1 - \delta - d_3) \cdot T] \quad (3.17)$$

Stage IV:

$S_1$  is on and  $S_3$  is off, this is charging mode when the solar system is capable of supplying the load independently and, in the meantime, charging the storage system.

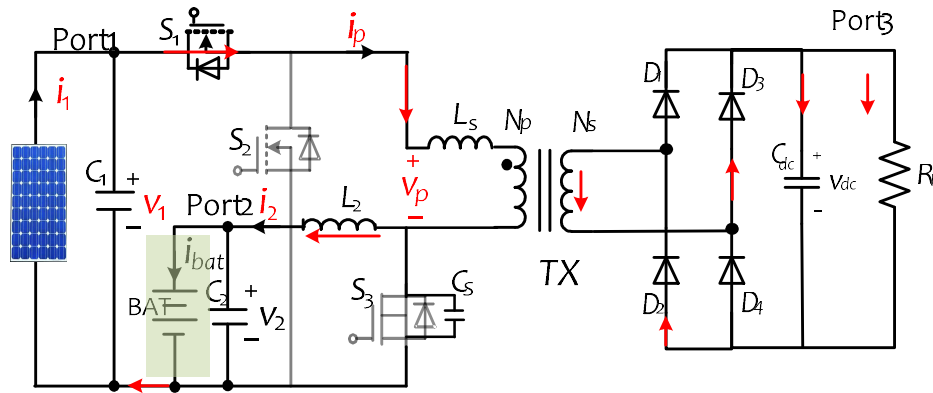


Figure 3.7 The operation states of the proposed converter Stage IV

$$\begin{cases} (L_s + L_m) \cdot \frac{di_p}{dt} = V_1 - v_{ds3} \\ L_2 \cdot \frac{di_2}{dt} = v_{ds3} - V_b \\ C_s \cdot \frac{dv_{ds3}}{dt} = i_p - i_2 \end{cases} \quad (3.18)$$

$$\begin{aligned} C_s \cdot \frac{dv_{ds3}^2}{dt^2} &= \frac{V_1 - v_{ds3}}{L_s + L_m} - \frac{v_{ds3} - V_b}{L_2} \\ &= -\left(\frac{1}{L_s + L_m} + \frac{1}{L_2}\right) \cdot v_{ds3} + \frac{V_1}{L_s + L_m} + \frac{V_b}{L_2} \end{aligned} \quad (3.19)$$

$L_m \gg L_2$ ,

$$L_2 \cdot C_s \cdot \frac{dv_{ds3}^2}{dt^2} + v_{ds3} \approx V_b \quad (3.20)$$

$$v_{ds3} = A \cdot \cos(\omega_{s2} \cdot t) + B \cdot \sin(\omega_{s2} \cdot t) + V_b \quad (3.21)$$

$d_{vds3}(0) = I_p - I_2$ ,

$$\dot{v}_{ds3} = \omega_{s2} \cdot V_b \cdot \delta \cdot T \cdot \cos[\omega_{s1} \cdot (1 - \delta - d_3) \cdot T] \quad (3.22)$$

$$\dot{v}_{ds3}(0) = \omega_{s2} \cdot V_b \cdot \delta \cdot T \quad (3.23)$$

$$\begin{cases} v_{ds3}(0) = A + V_b = V_T \\ \dot{v}_{ds3}(0) = \omega_{s2} \cdot B = \omega_{s2} \cdot V_b \cdot \delta \cdot T \end{cases} \quad (3.24)$$

$$v_{ds3} = (V_T - V_b) \cdot \cos(\omega_{s2} \cdot t) + V_b \cdot \delta \cdot T \cdot \sin(\omega_{s2} \cdot t) + V_b \quad (3.25)$$

The peak value of  $V_{ds3}$  is:

$$v_{ds3,\min} = V_b - \sqrt{(V_T - V_b)^2 + (V_b \cdot \delta \cdot T)^2} \quad (3.26)$$

The time duration is:

$$d_1 \geq \frac{\pi + \tan^{-1} \left[ \frac{(V_T - V_b)}{2\pi \cdot k_\omega \cdot V_b \cdot \delta} \right]}{2\pi \cdot k_\omega} + \delta \quad (3.27)$$

Then the ZVS condition is

$$\delta \geq \frac{\sqrt{2V_T \cdot V_b - V_T^2}}{2\pi \cdot k_\omega \cdot V_b} \quad (3.28)$$

### 3.3 Design Considerations

#### 3.3.1 ZVS analysis

The Phrases "hard switching" and "soft switching" relate to switching techniques that are dependent on the current-voltage relationship during the IGBT's on- and off-states.

Figure 3.8 (a) illustrates a typical hard-switching current, voltage waveforms, and operating zone. Voltage and current are applied to the device during on-off transitions. When collector current and collector-emitter voltage are switched forcefully, collector current and collector-emitter voltage change sharply, resulting in switching disturbance and losses. Hard switching is utilized in applications such as simple switches, motor drive inverters, and switched-mode power supplies. In comparison, soft switching uses an  $LC$  resonant circuit to turn a device on and off at zero current or voltage (ZVS or ZIS). Alternatively, the voltage and current switching timings are regulated so that the intersection of their waveforms is minimized.

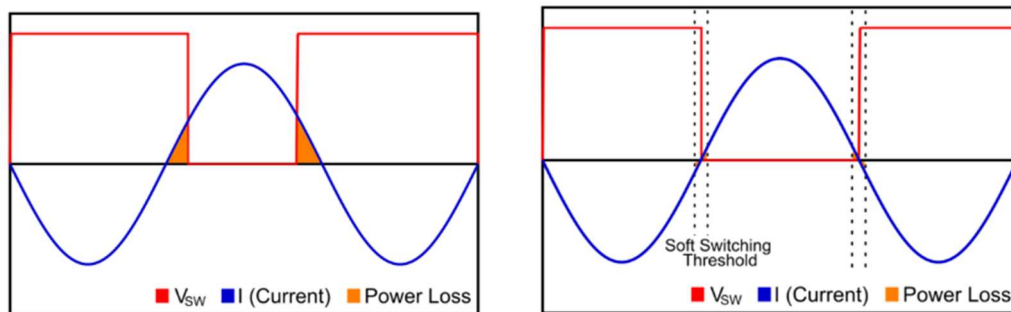


Figure 3.8 (a-b) shows hard and soft switching.

The current and voltage waveforms of a soft-switched device and its operational zone are shown in Figure 3.8(b). Because switching devices turn on and off at zero or virtually zero voltage or current, soft switching helps eliminate or reduce switching disturbance and losses. Soft switching is commonly in the power electronic devices such as Converters or inverters that because soft



switching offers more advantages in terms of protecting the sensitive small components. Also, in this converter and in the solar array system, batteries are essential, so charging and discharging the batteries are important and have a significant impact on the system's performance. The charge mode influences battery performance and efficiency, which is why the ZVS technique is essential.

### 3.3.2 Delta Calculation

$$\delta \geq \frac{1}{V_1} \cdot \underbrace{\sqrt{\frac{Z_s \cdot P_3}{\pi \cdot (1 - 2d_1)}}}_{\delta_{3c,m}} \quad (3.29)$$

$$\delta \leq d_1 - \underbrace{\frac{1}{\omega_{r2} \cdot T}}_{\delta_{3c,M}} \cdot \left( \frac{3}{2} \cdot \pi \right) \quad (3.30)$$

$Z_s = 2\pi \cdot f \cdot L_s$ . ( $f$  is the switching freq.,  $T = 1/f$ ),  $L_s = 4 \mu\text{H}$  if A transformer is used,  $P_3$  is the power at the secondary side.

$$\omega_{r2} = \frac{1}{\sqrt{L_2 \cdot C_s}} \quad (3.31)$$

$L_2 = 470 \mu\text{H}$ ,  $C_s = 4 \text{ nF}$

The ZVS range of  $S_3$  is  $\delta_{3c,m} \leq \delta \leq \delta_{3c,M}$ , therefore, for (1),  $d_1$  should be set less than 0.6, the smaller the better, for example,  $d_1 = 0.42$ , the value of  $\delta$  is set the middle value of  $\delta_{3c,m}$  and  $\delta_{3c,M}$  around 0.2.

### 3.3.3 Maximum Power Point Tracking of PV System

In a PV system, the load characteristics changes to provide the maximum power from the system; this optimal load characteristic is known as the maximum power point. Maximum power point tracking is referred to the algorithm which is used in the controller to draw the maximum power available from PV under certain conditions. The PV cell has a nonlinear power curve due to the non-linear relationship between temperature and total resistance, the best way to analyze the PV cell power is the current voltage relationship where the maximum voltage is the open circuit voltage, and the maximum current is the short circuit current. The voltage at which the PV module can produce the maximum power is called maximum power point (or peak power voltage). Solar radiation, ambient temperature, solar cell temperature, as well as the age of the cell are some common conditions that affect the maximum power of the solar cell. Figure 3.9 below shows the current voltage curve for maximum power point tracking, where at the maximum power point, the voltage is  $V_{mp}$  and the current is  $I_{mp}$ ,  $I_{sc}$  is the short circuit current and  $V_{oc}$  is the open circuit voltage.

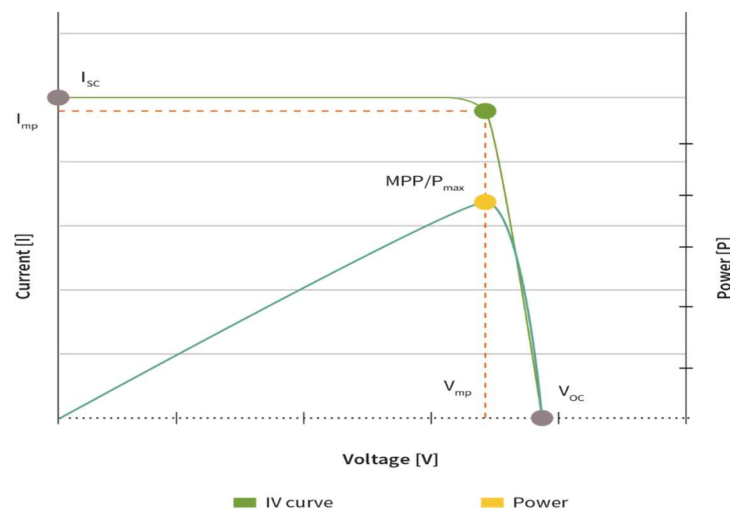


Figure 3.9 MPPT Controller tracking the power curve of the solar

There are a varieties of algorithms that can be used for maximum power point tracking, I have used a straightforward algorithm which will track the first maximum power point only. The flow chart below shows the algorithm, wherein the primary state, we consider the current  $I(K)$  and the voltage  $V(K)$  of that instant, and by multiplying the two values, we get the first power primary  $P(K)$ . For the next instant, we take the voltage and current for that instant and get the power by the same process.

Now the second power, which is the current instant is our  $P(K)$  value, and the power we have calculated at the first time is our previous value denoted as  $P(K-1)$ .

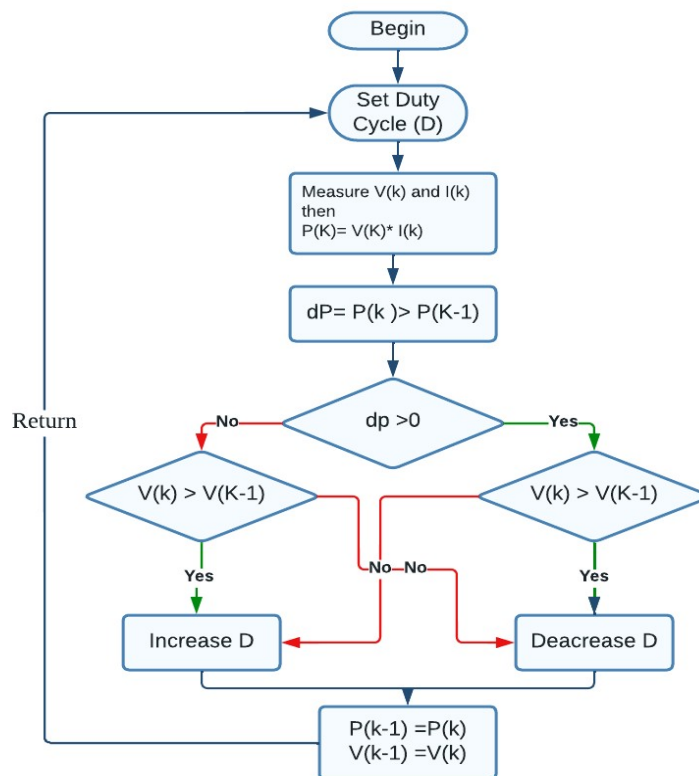


Figure 3.10 MPPT flow chart

Then the algorithm examines if the current power is higher than the previous power by subtracting the previous one from the current value, which is denoted by  $dP$ , if the result of the subtraction is  $dP$  greater than 0, that means the current power is greater than the previous state of power.

Following that, we check whether the current voltage is higher or lower than the previous state voltage since we can control the voltage by controlling the duty cycle. If the current voltage is higher than the previous stage voltage, we decrease the duty cycle  $d$ , if it is lower than the previous stage, we increase the duty cycle  $d$ . If  $dP$  is not greater than 0, then we follow the opposite path, as shown above in Figure 3.10.

## Chapter 4 Simulation and Experimental Validations

### 4.1 Simulation

The presented model is simulated in MATLAB/Simulink using an inbuilt solar panel from Advance Solar Hydro Wind Power API 150. Table 4.1 specifies the values of the parameters used and the solar panel. A 30V, 12Ah lead acid battery is under consideration. The MIC's switching frequency has been set to 20 kHz. The model is simulated under various conditions and modes, as explained in the previous chapters, operation principle and the stages section.

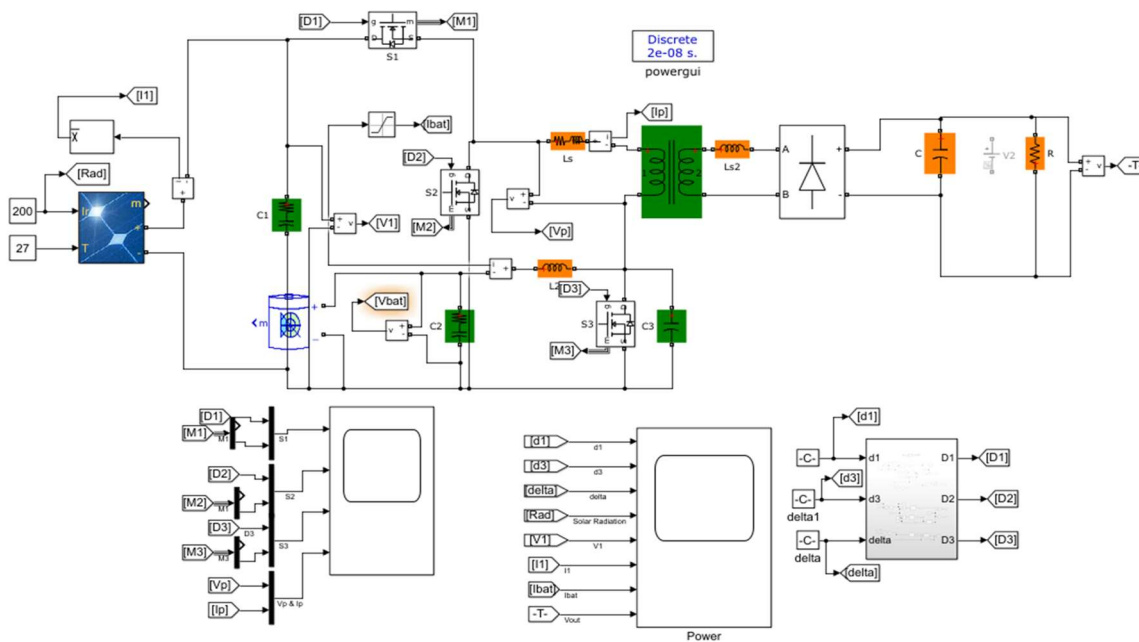


Figure 4.1 The built simulation circuit of the TPC

The simulation follows the duty cycle for the switching for S3, which is charging and discharging the battery in two different working modes. Here the blue signal is the voltage across the S3, and the yellow signal represents the current across the switch. Also, the yellow signal shows the switching, and the objective is getting the zero-voltage switching.

From the figure 4.2 below we can see that our simulation is almost reached close to the zero-voltage switching which will help us to achieve zero loss during the transformation. This data is validated and will be shown in the Laboratory setup and validation.

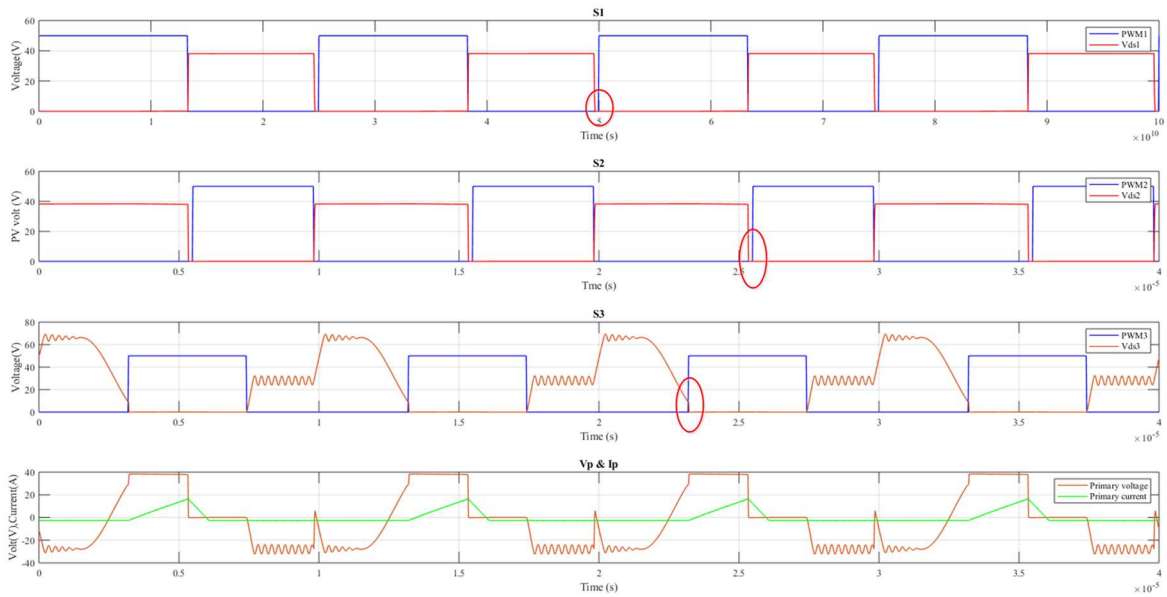


Figure 4.2 illuminates the simulation ZVS.

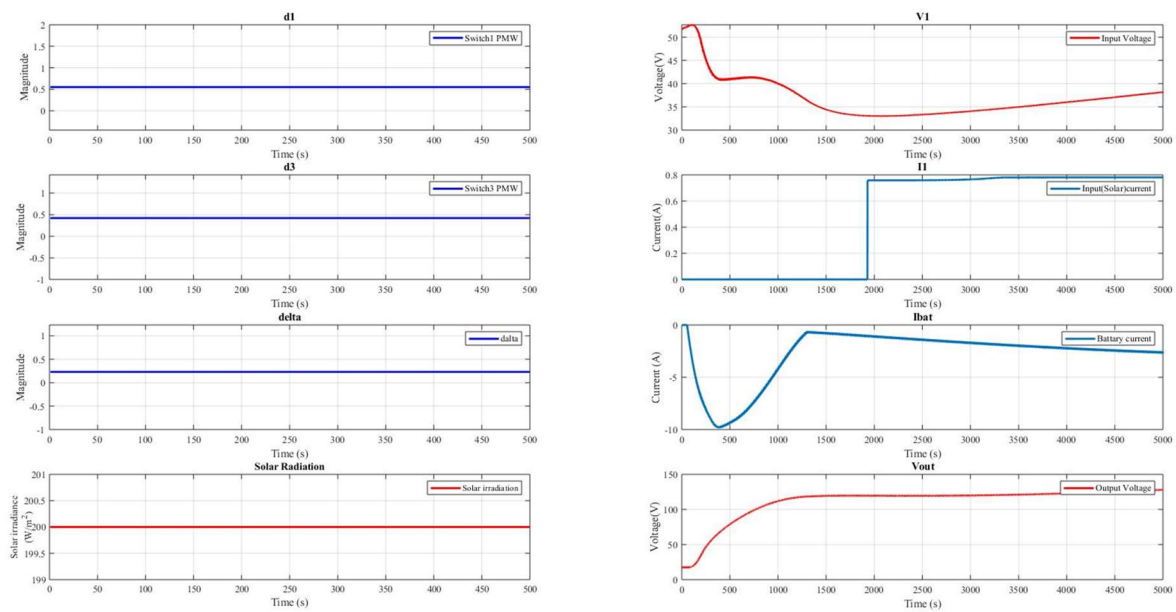


Figure 4.3 Simulation waveforms.

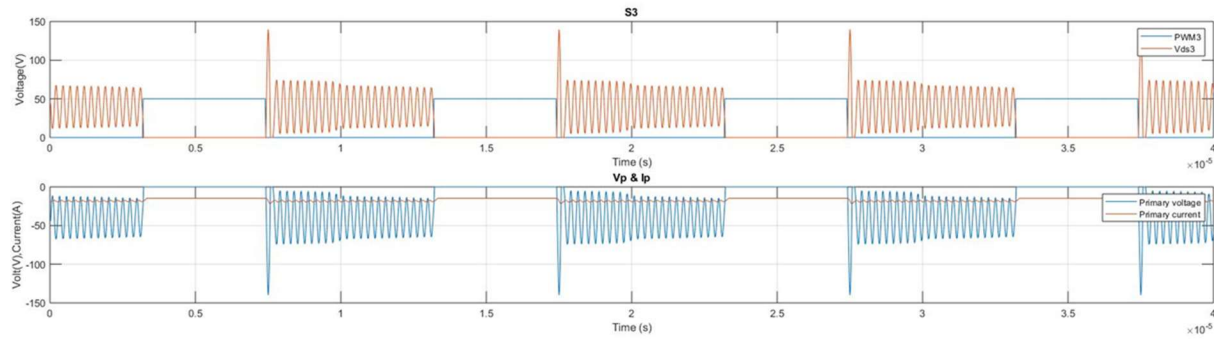


Figure 4.4 Demonstration of the ZVS at switch3

## 4.2 Laboratory Setup

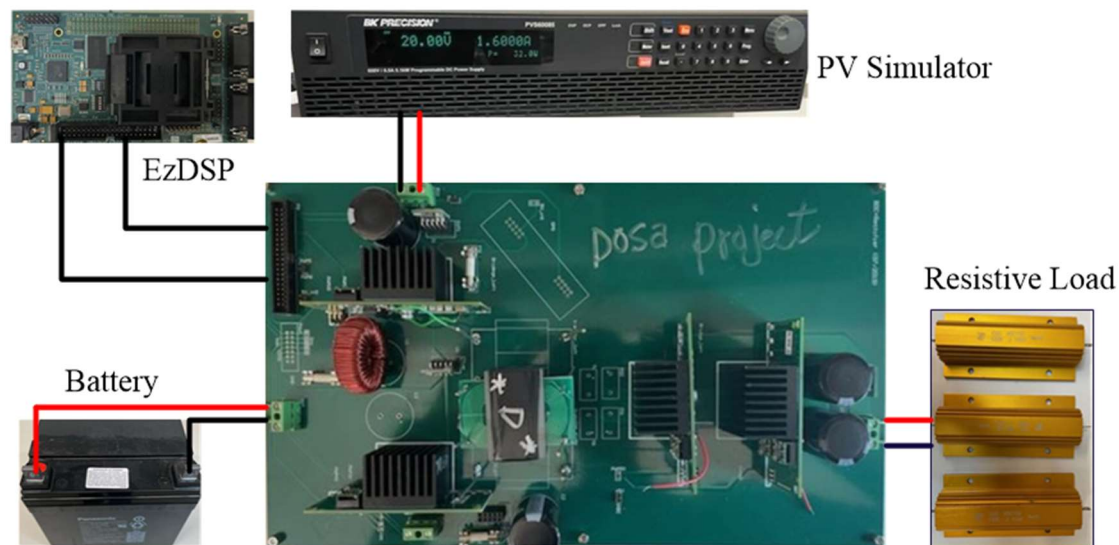


Figure 4.5 Experimental system setup

A 500W prototype is realized in hardware to validate the proposal converter, all real-time control algorithms have been implemented in an eZdsp F28335 control board, and then we generated the pulse generation module of the MOSFETs all the pulses are at 50% duty cycle, the converter parameters are given in Table 4.2. The battery port has three 12V, 12Ah lead acid batteries connected in parallel with switch two. Port one uses a BK PVS60085MR PV simulator

with a magnitude of 30V, to emulate a renewable energy source (V1). Port three is connected to resistive load as shown in Figure 4.5 above, the converter operates in a closed loop with output voltage regulated around 65V.

Table 4.2 the proposed converter parameters

Converter Parameters	Value
L2	470 uH
Ls	6.4 uH
C1, C2	330 uF
Cs3	2.2 nF
Cdc	330 uF

### 4.3 Transformer Design and Calculation of Leakage Inductance

The planar transformer continues to develop as an alternative to wire-wound transformers. A wire-wound transformer has each winding wound on a separate soft iron limb or core. A planar transformer is simply a transformer that creates the coils out of flat windings, typically on a PCB board. It makes it perfect in some applications for improved efficiency and performance as well as compactness. The PCB construction produces a distinct form factor that not only saves time, money, and space but also perfectly satisfies individual requirements. There are four types of “transformer construction” and designs available with the different order of the PCB board, shown as Figure 4.6 Case-a is a fully interleaved winding configuration; case-b and case-c are partially interleaved winding non-interleaved winding configurations are used in case d setups.



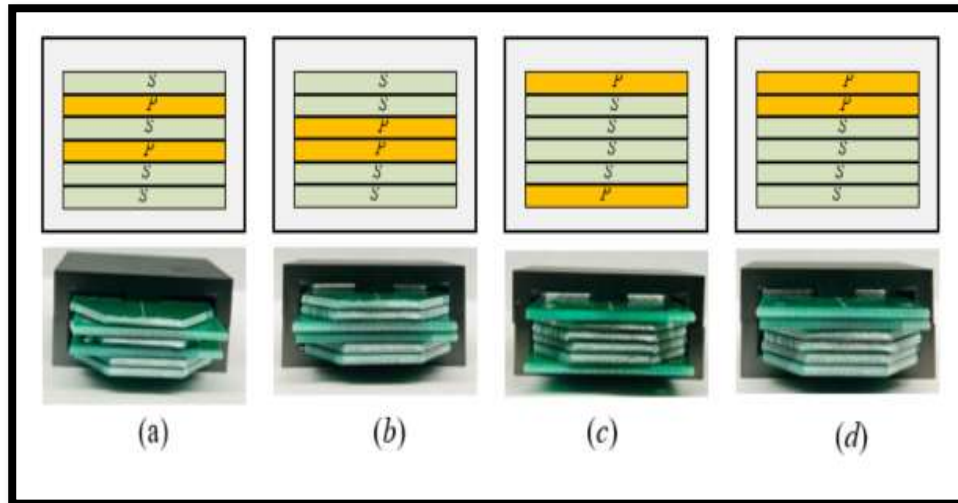


Figure 4.6 Different configurations of Transformer winding.

The primary and secondary sides of each of these planar transformers are wound with six turns each with two winding portions and fourteen turns each with four winding portions. That results in a theoretical turn ratio of 4.67 for each transformer.

A transformer's leakage inductance, an inductive component, is created when two windings are not perfectly magnetically connected. 100% of the energy is magnetically linked from the primary to the secondary windings in a perfect transformer. The signal created in the secondary windings is lessened by imperfect coupling. Any magnetic flux acting in series with the primary winding but not connecting it to the secondary winding is regarded as inductive impedance.

As a result, this "leakage inductance" is depicted on a schematic diagram as an extra inductance placed before the primary of an ideal transformer that is shown in the proposed TPC topology.

Leakage inductance should be low enough when it is undesirable in a wound component in some applications. Still, it must make up a more significant fraction of the total inductance to provide the energy storage medium required to ensure proper circuit performance. The transformer's leakage inductance value must be understood to be within predetermined bounds.

In some transformer designs, adding an air gap to the core or utilizing non-interleaved windings are typically used to produce a higher amount of leakage inductance [35]. The waveform of the transformer's primary voltage and current displayed in Figure 4.7 can be used to compute the leakage inductance value. The following differential equation can be derived for the transformer:

$$\begin{cases} v_p = L_{s1} \frac{di_p}{dt} + v_T \\ n \cdot v_T = v_s \end{cases} \quad \text{Thus}$$

$$L_{s1} = \frac{V_{p1} - V_{s1}/n}{di/dt}$$

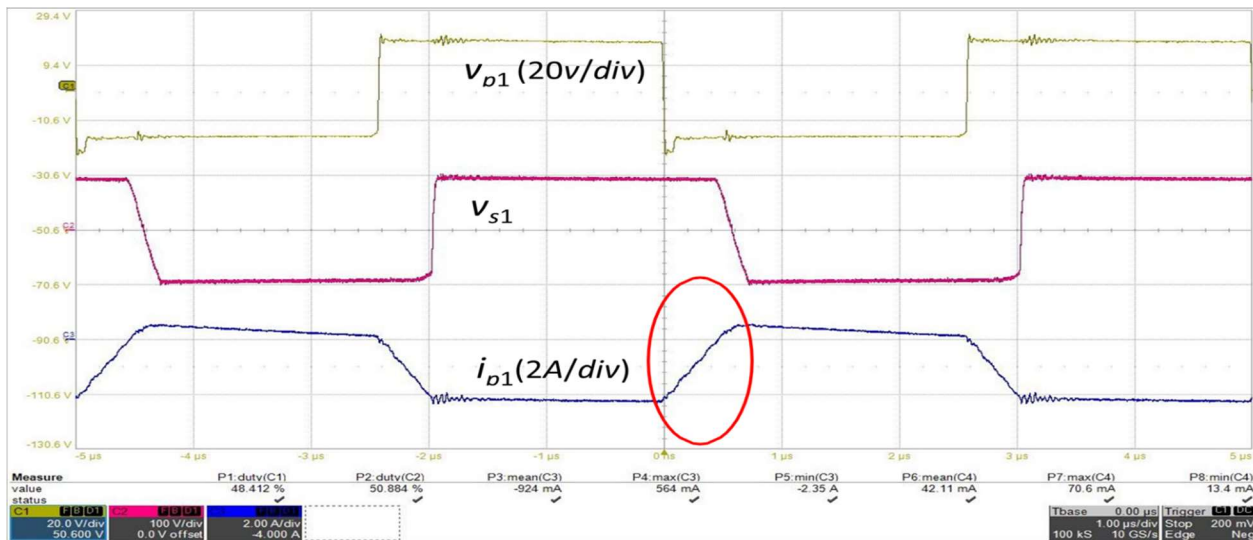


Figure 4.7 Inductance leakage waveform calculation [33].

leakage Inductance for type A	$L_{c\_a}$	1.63 uH
leakage Inductance for type B	$L_{c\_b}$	2.3 uH
leakage Inductance for type C	$L_{c\_c}$	4.3 uH
leakage Inductance for type D	$L_{c\_d}$	6.4 uH

The above table shows the leakage inductances and parameters for these four types of transformer construction in the lab. Case-A non-interleaved winding configurations were used in the experiment. The initial core permeability is 2300 and the core material is Ferrite Cores 98 with a turn ratio of 56:12.

#### 4.4 Experiment Results

To validate the theory of the ZVS analysis, the prototype circuit powered up. Java signal code was built in MATLAB and then compiled and loaded into eZdsp F28335 control to generate PWM in the circuit. Output waveforms are recorded when the converter works in the three modes mentioned in chapter 2 from the primary/secondary side of the transformer, and the input/output voltage as well as the ESS current all the result was consistent with the simulation result.

When the PV produces more power than the load needs ( $P_{Pv} > P_{Ld}$ ), then the extra energy will be used to charge the batteries ( $P_{Pv} - P_{Ld}$ )  $P_B > 0$ ,  $P_{Pv} = P_B + P_{Ld}$  that calls the charging mode.

Figure 4.8 shows the pulse width modulation (PWM) for  $S_1$  and  $S_3$ , where the phase shift  $\delta$  is 0.5, and shows the transformer voltage and current of the primary side.

The experiment results, as shown in Figure 4.9 and Figure 4.10, proved that the switches  $S_1$  and  $S_3$  can achieve ZVS at any value of  $\delta$ , which is compatible with the calculation.

Figure 4.11 shows the input voltage and current collected by the PV, the charging current and the converter's output voltage.

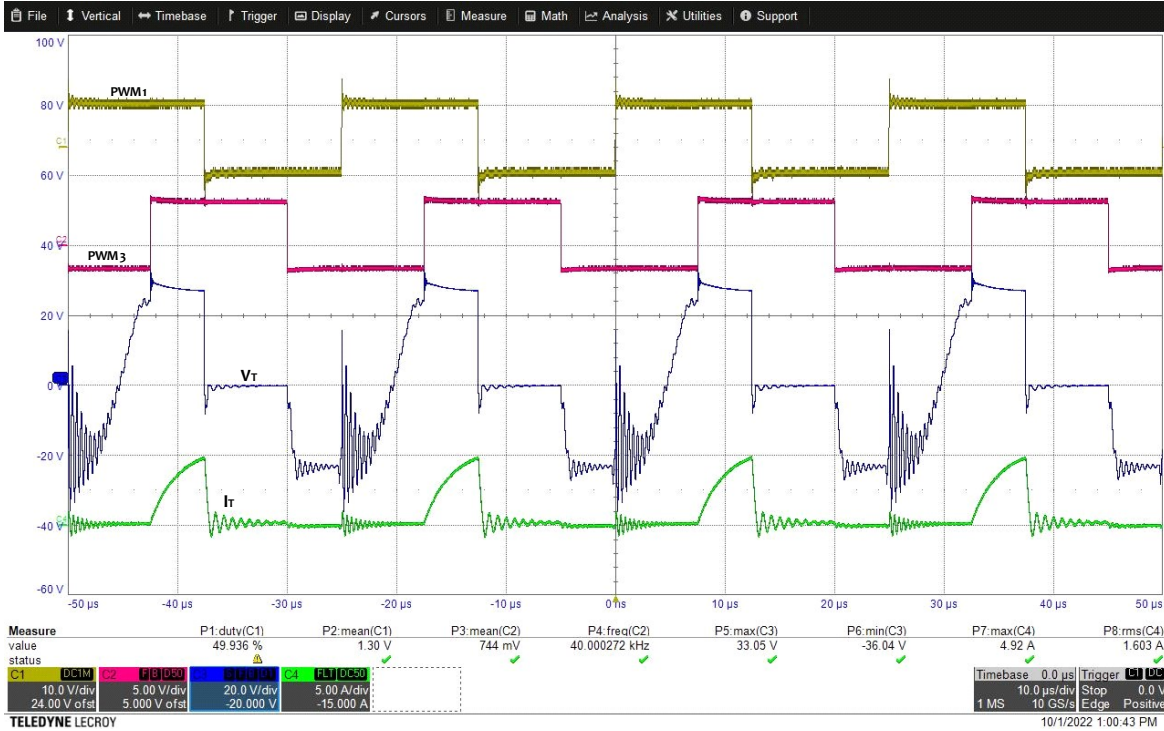


Figure 4.8 Measured waveform of  $V_T$  &  $I_T$  when the PV panel connects to the TPC

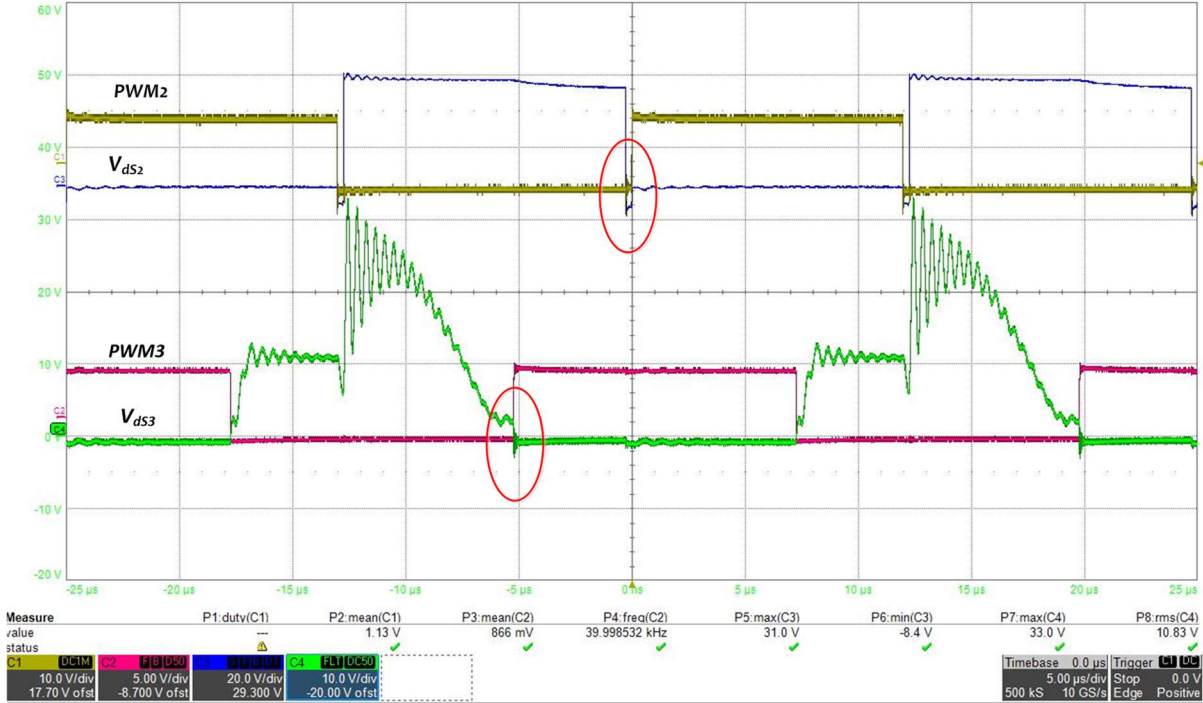


Figure 4.9 Measured waveform of  $V_{ds1}$  &  $V_{ds3}$  when the PV panel connects to the TPC.

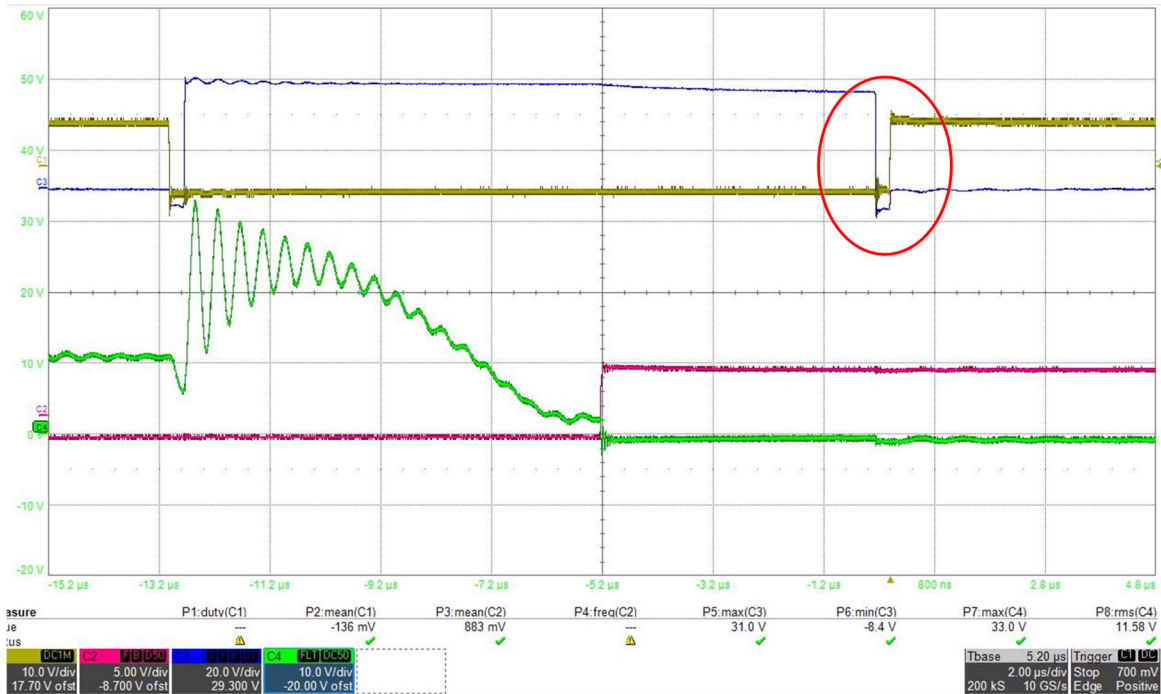


Figure 4.10 Measured waveform of  $S_1$  &  $S_3$  working under ZVS when PV is the source &  $\delta$  is 0.5.

When the PV produces power less than the load needs ( $P_{Pv} < P_{Ld}$ ), then the battery discharge power to compensate the power shortages in the circuit, which call discharging mode or the battery delivery mode  $P_{Ld} = P_B + P_{Pv}$ .

Figure 4.12 and Figure 4.13 show the pulse width modulation (PWM) for  $S_1$  and  $S_3$ , where the phase shift  $\delta$  is 0.23, and show the voltage of the two switches ( $V_{S1}$  &  $V_{S3}$ ). And current. Figure 4.14 shows the contribution of the two power sources ( $V_{Pv}$ ,  $I_{Pv}$ ,  $I_b$ ) and the  $V_{dc}$  output voltage.

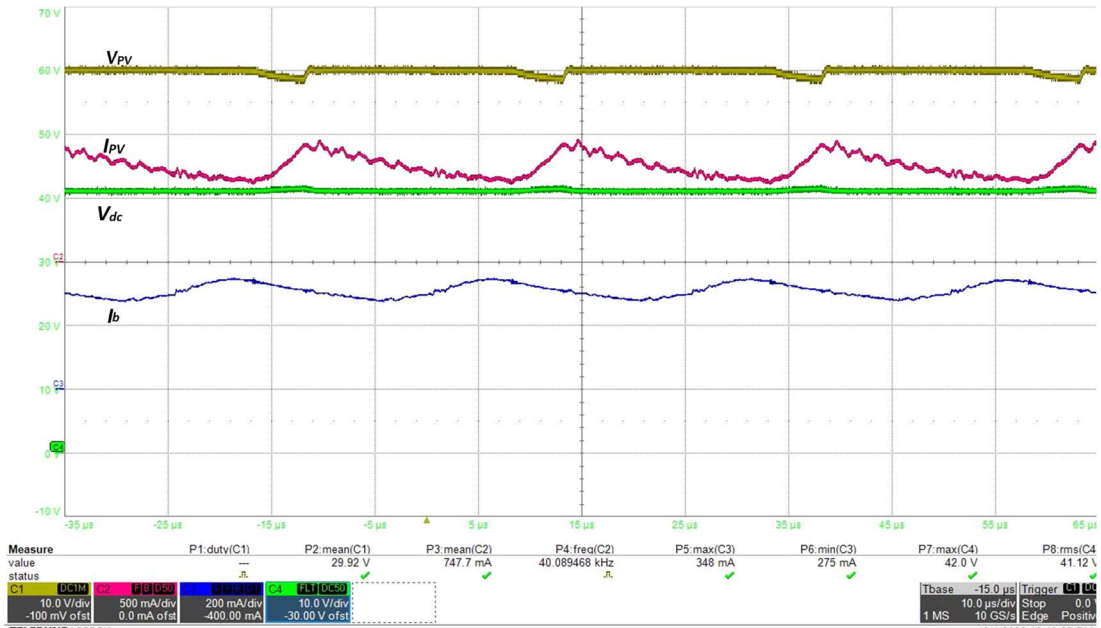


Figure 4.11 Measured waveform of the  $V_{pv}$ ,  $I_{pv}$ ,  $I_b$  &  $V_{dc}$  when the load is connected.

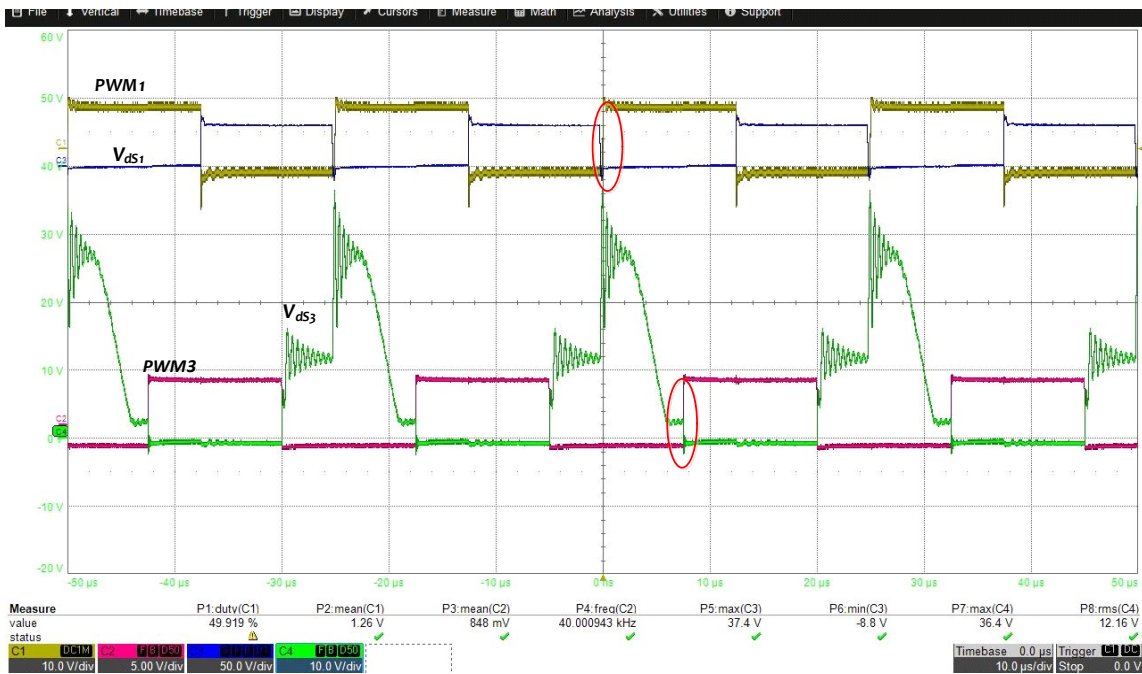


Figure 4.12 Measured the PWM of  $S_1$ ,  $S_3$ ,  $V_{s1}$  &  $V_{s3}$  in the deliver mode when  $\delta$  is 0.23.

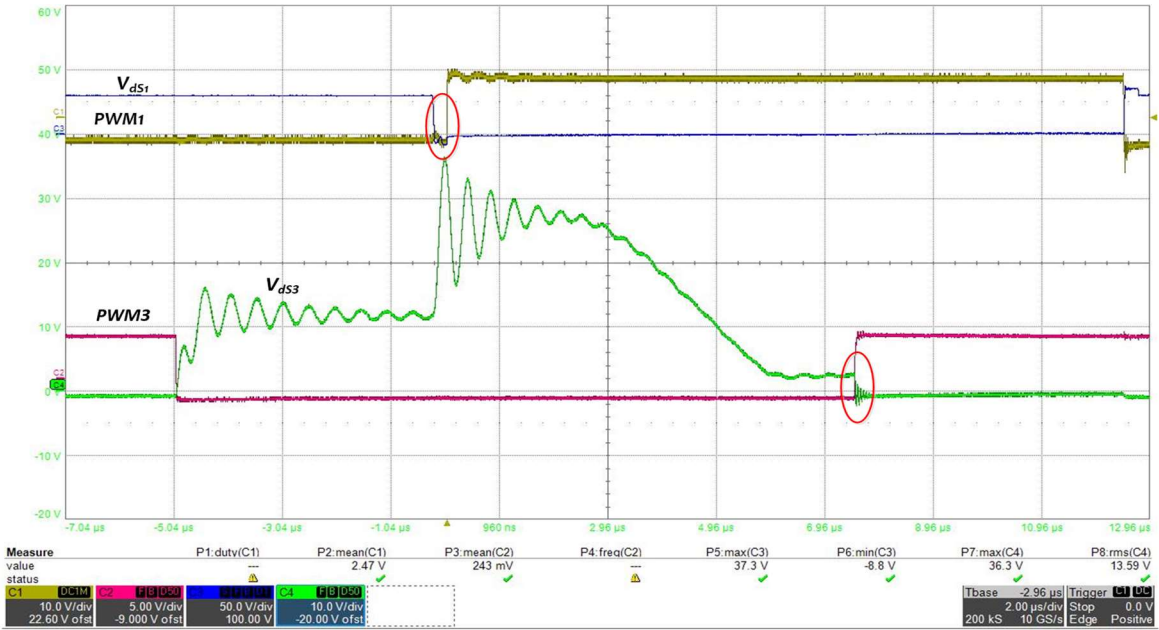


Figure 4.13 shows  $S_1$  and  $S_3$  ZVS when TPC is in the delivery mode.

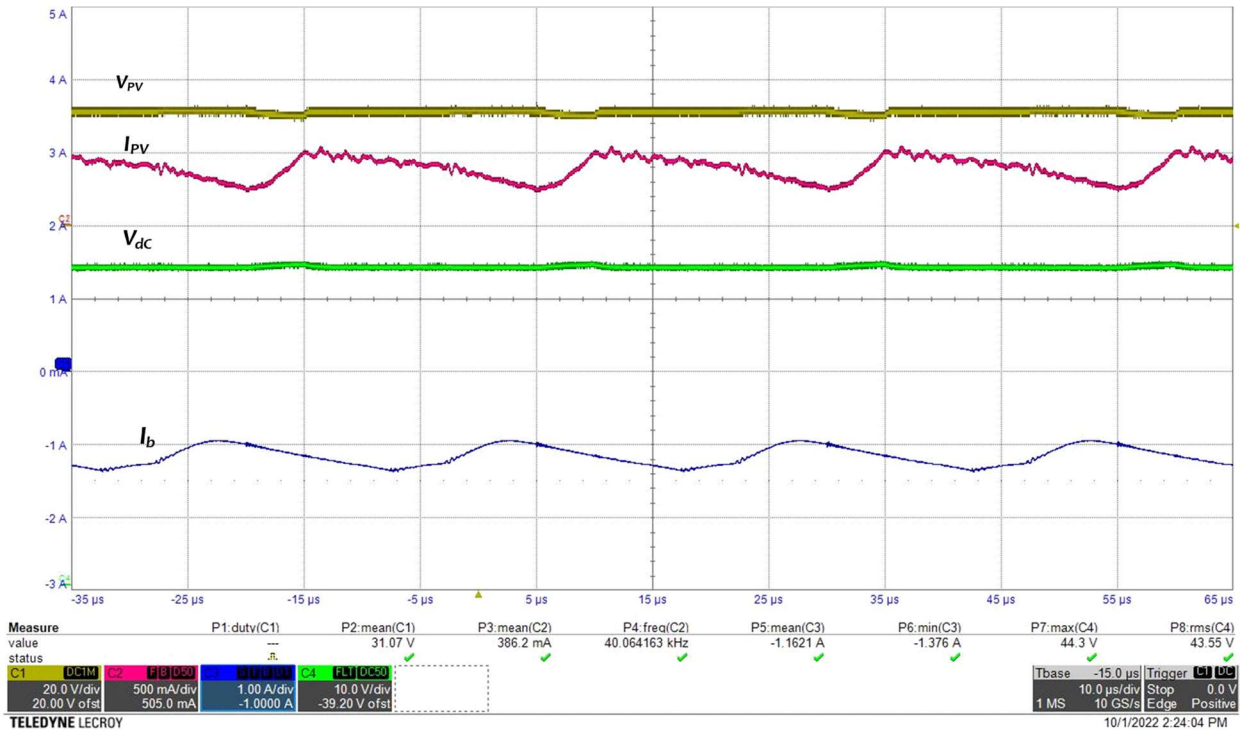


Figure 4.14 Measured waveform of the PV volt/current, battery current & output voltage.

When the PV is not producing any energy ( $P_{Pv} = 0$ ) at night, for example, the battery will take over the load  $P_{Ld} = P_B$ , Figure 4.15 shows the pulse width modulation (PWM) for  $S_1$  and  $S_3$ , where the phase shift  $\delta$  is 0.25, in addition to the voltage and the current of the transformer ( $V_T$ ,  $I_T$ ). It's proven the theoretical concept of the ZVS in this mode for the converter.

The theoretically critical ZVS condition of  $S_3$  is  $\delta = 0.538$ , which agrees with the experiments in the range of the allowable error. As shown in the Figure 4.16 below, before the gate signals PWM1 and PWM3 are applied,  $v_{ds1}$  and  $v_{ds3}$  have already dropped to zero, which indicates  $S_1$  and  $S_3$  are turned ON under the ZVS condition. Thus, the ZVS theoretical calculation is verified by the experiments.

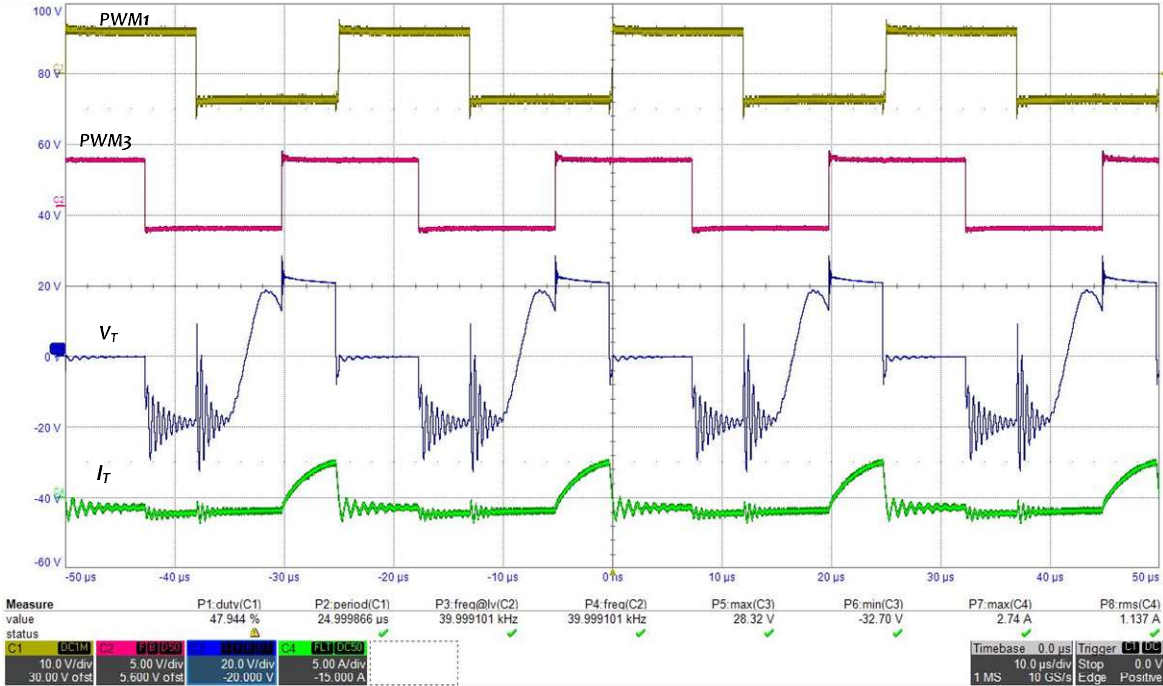


Figure 4.15 Measured waveform of the transformer voltage and current in SISO mode.



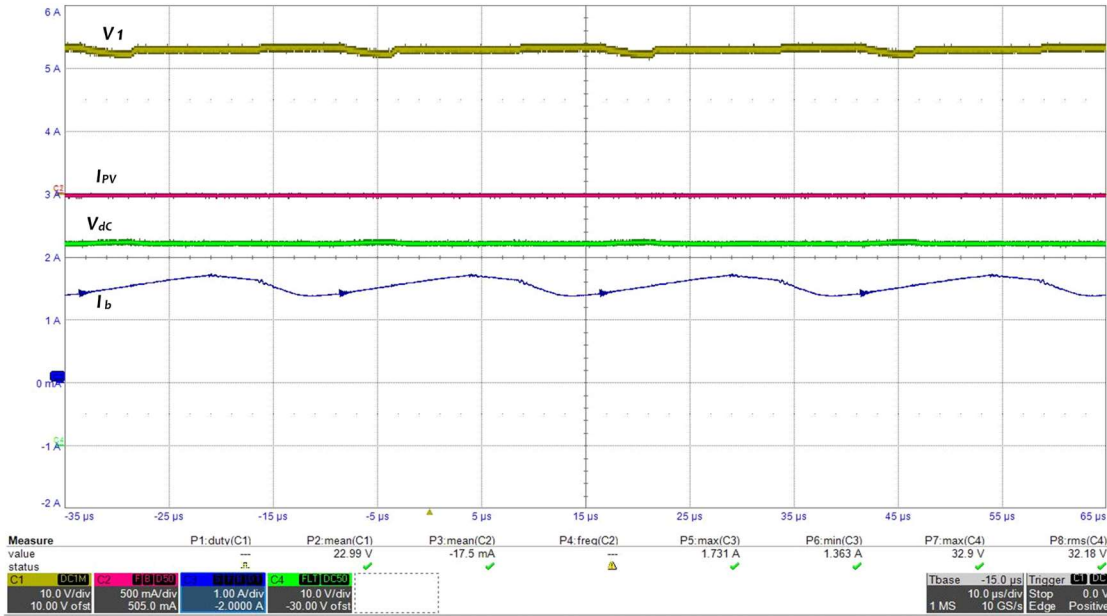


Figure 4.16 Measured waveform of the input/output voltage of the SISO mode.

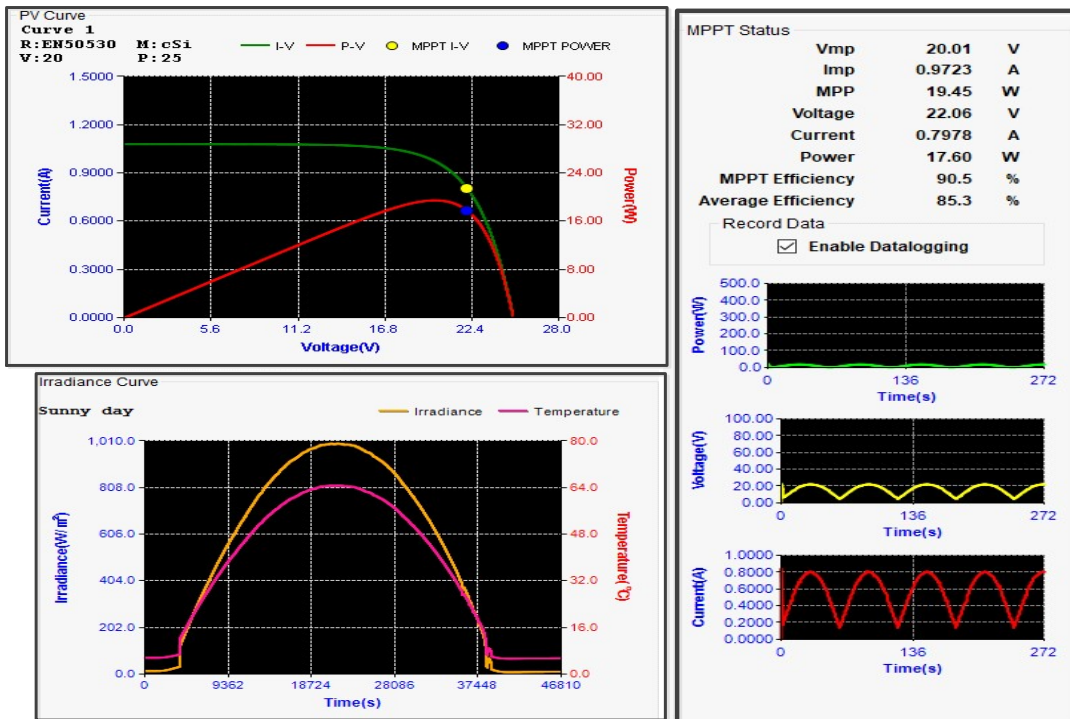


Figure 4.17 shows the PV simulator parameters.

## Chapter 5 Conclusion, Recommendation for future work

### 5.1 Conclusion

Solar panels are examples of renewable energy sources that are being employed in stand-alone applications in the home, business, and automotive. Multi-port dc-dc converters are required to connect the sources and the load in these applications, together with energy storage.

This thesis presents three port Dc-Dc converter designed to power managing solar panel sources with battery and DC micro-grid system. There are some advantages to this proposed converter, and more goals were achieved during the research phase.

- Design that is inexpensive and effective, by using a smaller number of switches while maintaining the ZVS performance to minimize the power losses in the system.
- Maximum power point tracking of the solar achieved, the converter working with high efficiency by using MPPT that, also demonstrated in the simulation and the validation.
- Operation modes, the converter is capable of working in different operating modes, and regardless of RES availability or load demand, the converter is capable of controlling energy flow in the system.
- The proposed converter has verified that it works efficiently in all the different modes

All the above results have been simulated using MATLAB Simulink and validated using the experiment prototype, the result shows that the simulation and the experimental values are a 90% match.

## 5.2 Recommendations for Future Work

Although the proposed converter may set the trend for multiport converters, several issues remain unresolved, motivating future improvements and research into existing controllers and integrated systems. Several potential improvements remain to research which are listed below.

- Study the transient response, dynamic response and the steady state response of the converter and observe the effect on the efficiency and sustainability of the converter output as well as the soft-switching technique.
- Built controller to the converter and integrated it to multiport converters, suggesting that Sooner, multiport converters will be widely used in homes and buildings, making each house, or building a small micro-grid. It is important to study and comprehend how to connect them to the grid and unify and regulate the group operation management.
- Integrate micro-grids that can utilize several sources and are capable of supplying a single household as well as a small community and adding a rechargeable battery will allow providing power continuously during day and night.

## References

- [1] Ajay Kumar, Nitin Gupta and Vikas Gupta, "A Comprehensive Review on Grid-Tied Solar Photovoltaic System," *Journal of Green Engineering*, pp. 213-254, April 2017.
- [2] Xi Lu, Michael B. , and Juha Kiviluoma, "Global potential for wind-generated electricity," *PNAS*, p. 6, July 2009.
- [3] O. Rubanenko, V. Yanovych, O. Miroshnyk and D. Danylchenko, "Hydroelectric Power Generation for Compensation Instability of Non-guaranteed Power Plants," in *2020 IEEE 4th International Conference on Intelligent Energy and Power Systems (IEPS)*.
- [4] M. S. P. Adhau, R. M. Moharil and P. G. Adhau, ""Estimation of micro hydro power plant capacity from potential sites," in *2012 IEEE International Conference on Power Electronics, Drives and Energy Systems (PEDES)*, Bengaluru, India , 2012.
- [5] N. Anku, J. Abayatcye and S. Oguah, "Smart grid: An assessment of opportunities and challenges in its deployment in the ghana power system," in *2013 IEEE PES Innovative Smart Grid Technologies Conference (ISGT)*, Washington DC.
- [6] H. Weiss, T. Winkler and H. Ziegerhofer, "Large lithium-ion battery-powered electric vehicles — From idea to reality," in *2018 ELEKTRO*, Mikulov, 2018.

- [7] R. Fatima, A. A. Mir, A. K. Janjua and H. A. Khalid, "Testing study of commercially available lithium-ion battery cell for electric vehicle," in *2018 1st International Conference on Power, Energy and Smart Grid (ICPESG)*, Mirpur, 2018.
- [8] "The role of microgrids in enhancing macrogrid resilience," in *2016 International Conference on Smart Grid and Clean Energy Technologies (ICSGCE)*, Chengadu, 2016.
- [9] Xuan Liu, Bin Su, "Microgrids - An Integration of Renewable Energy Technologies," Corporate Research, ABB (China) Limited, Beijing.
- [10] Dugan R., Mark McGranaghan, *Electric Power Systems Quality 2nd Edition*, 2003.
- [11] "U.S. Energy Information Administration," Dec. 2021. [Online]. Available: <https://www.eia.gov/energyexplained/electricity/electricity-in-the-us.php>.
- [12] Sun Kai, Zhang Li, Xing Yan, Guerrero Josep M., "A Distributed Control Strategy Based on DC Bus Signaling for Modular Photovoltaic Generation Systems With Battery Energy Storage," *IEEE Transactions on Power Electronics*, 2011.
- [13] Neng Zhang n , Danny Sutanto, Kashem M. Muttaqi, "A review of topologies of three-port DC–DC converters for the integration of renewable energy and energy storage system," *Renewable & Sustainable Energy Reviews*, 2015.
- [14] Zhiqing Wang , Quanming Luo, Yuqi Wei, Di Mou, Xinlei Lu, and Pengju Sun, "Topology Analysis and Review of Three-Port DC–DC Converters," in *IEEE TRANSACTIONS ON POWER ELECTRONICS*, 2020.

- [15] S. A. Abdelrazek and S. Kamalasadán, "Integrated PV capacity firming and energy time shift battery energy storage management using energy-oriented optimization," in *IEEE Trans. Industry Appl*, June 2016.
- [16] Wu H, Sun K, Ding S, Xing Y., "Topology derivation of non-isolated three-port DC–DC converters from DIC and DOC," in *IEEE Trans Power Electron* , 2013.
- [17] Chen YM, Huang AQ, Yu X., "A high step-up three-port DC–DC converter for stand-alone PV/Battery power systems," in *IEEE Trans Power Electron 2013*, 2013.
- [18] Ding S, Wu H, Xing Y, Fang Y, Ma X., "Topology and control of a family of non-isolated three-port DC/DC converters with a bidirectional cell," 2013.
- [19] Vazquez N, SanchezCM, Hernandez C, Vazquez E, Lessó R., "A three-port converter for renewableenergy applications," in *2011 IEEE International Symposium on Industrial Electronics*, 2011.
- [20] Chen Y, Wen G, Peng L, Kang Y, Chen J., "A family of cost-efficient non-isolated single-inductor three-port converters for low power standalone renewable power applications," in *2013 Twenty-Eighth Annual IEEE Applied Power Electronics Conference and Exposition (APEC)*, 2013.
- [21] Chen Y, Zhang P, Zou X, Kang Y. , "Dynamical modelling of the non-isolated single-inductor three-port converter," in *2014 Twenty-Eighth Annual IEEE Applied Power Electronics Conference and Exposition (APEC)*, 2014.

- [22] Zhu H, Zhang D, Zhang B, Zhou Z. , "A non-isolated three-port DC–DC converter and three-domain control method for PV-battery power systems," in *IEEE Trans Ind Electron* 2015, 2015.
- [23] Alves DBS, Praca Jr. PP, Oliveira DS, Barreto LHSC, de Freitas LCG., "A single-stage three-port boost converter with high voltage gain based on the bidirectional version of the three-state switching cell," in *2015 Twenty-Eighth Annual IEEE Applied Power Electronics Conference and Exposition (APE)*, 2015.
- [24] Qian Z, Rahman OA, Al-Atrash H, Batarseh I, "Modelling and control of three- port DC/DC converter interface for satellite applications," in *2010 IEEE Trans Power Electron*, 2010.
- [25] QianZ, Rahman OA, Reese J, Atrash HA, Batarseh I, "Dynamic analysis of three- port DC/DC converter for space applications," in *2009 Twenty-Fourth Annual IEEE Applied Power Electronics Conference and Exposition*, 2009.
- [26] Sun X, Liu F, Xiong L, Wang B., "Research on dual buck/boost integrated three- port bidirectional DC/DC converter," in *2014 IEEE Conference and Expo Transportation Electrification Asia-Pacific*, 2014.
- [27] Wu H, Xing Y, Chen R, Zhang J, Sun K, Ge H., "A three-port half-bridge converter with synchronous rectification for renewable energy application," in *2011 IEEE Energy Conversion Congress and Exposition*, 2011.

- [28] Wu H, Chen R, Zhang J, Xing Y, Hu H, Ge H., "A family of three-port half-bridge converter for a stand-alone renewable power system," in *2011 IEEE Trans Power Electron*, 2011.
- [29] Zhu H, D. Zhang, H. S. Athab, B. Wu, and Y. Gu., "PV isolated three-port converter and energy-balancing control method for PV-battery power supply applications," in *IEEE Transactions on Industrial Electronics*, 2014.
- [30] R. D. K. J. Zhao C, "An isolated three-port bidirectional DC–DC converter with decoupled power flow management," in *IEEE Trans Power Electron*, 2008.
- [31] D. J. H. M. Tao H, "Three-port triple-half-bridge bidirectional converter with zero-voltage switching," in *IEEE Trans Power Electron* 2008, 2008.
- [32] B. S. F. Samavatian V, "A. Half-bridge current-fed multi-resonant bidirectional three-port DC converter for flexible distributed generation," 2014.
- [33] J. Zeng, X. Du, and Z. Yang, "A multiport bidirectional DC–DC converter for hybrid renewable energy system integration," *IEEE Trans. Power Electron.*, vol. 36, no. 11, pp. 12281-12291, Nov. 2021.
- [34] D. M. N. Biswas, "A three-port bidirectional DC-DC converter with zero-ripple terminal currents for PV/ microgrid applications," in *IECON*, 2013.



- [35] X. Z. W. J. W. V. & Y. Q. Du, "A four-port bidirectional DC-DC converter for renewable energy system and microgrid," Minnesota State University, Mankato, Mankato, MN , 2020.
- [36] Bethel Afework, Microgeneration Alberta, Jordan Hanania, Braden Heffernan, James Jenden, "Energy Education," Photovoltaic system, 2020. [Online]. Available: [https://energyeducation.ca/encyclopedia/Photovoltaic\\_system](https://energyeducation.ca/encyclopedia/Photovoltaic_system). [Accessed 2021].
- [37] M. Villalva, J. Gazoli, E.Filho, "Comprehensive Approach to Modeling and Simulation of Photovoltaic Arrays," *IEEE Transactions on Power Electronics*, pp. 1198-1208, May 2009.
- [38] H. Wu, P. Xu, H. Hu, Z. Zhou, and Y. Xing, "Multiport converters based on integration of full-bridge and bidirectional DC–DC topologies for renewable generation systems," in *2014 IEEE Trans. Ind. Electron*, Feb. 2014.
- [39] Wang and H. Li, "An integrated three-port bidirectional DC–DC converter for PV application on a DC distribution system," in *2013 IEEE Trans. Power Electron*, Oct. 2013.
- [40] B. S. F. A. Samavatian V, "Half-bridge current-fed multi- resonant bidirectional three-port DC converter for flexible distributed generation," in *Proceedings of PEDSTC*, 2014.

## Appendix(A)

### ZVS Analysis Code:

```

clear all; close all; clc;
Param_TPC; d3 = 0.5; Cs = 2.68e-6;
V1 = 55; Vdc = 180; VT = Vdc/n; d1 = Vb/V1;
%% ZVS of S3
P3 = 50; delta = 0.1:0.01:0.4;
VT = V1 - Zs*P3./(pi*delta.^2*V1);
Vds3 = Vb - sqrt( (VT - Vb).^2 + (Vb*delta*T).^2 );

alpha = atan( (VT - Vb)./(Vb*T*delta) );
delta3m = sqrt( Zs*P3./(pi*(1 - 2*d1)))/V1;
delta3M = d1 - (3*pi/2 - alpha)./(wr2 * T);          % S3
Idx = find( (delta >= delta3m) & (delta <= delta3M) );

% plot(delta,Vds3,'b-'); return;

%% ZVS of S3 -- 3D
[P3,delta] = meshgrid([20:2:100],[0.05:0.005:0.25]);
VT = V1 - Zs*P3./(pi*delta.^2*V1);
Vds3 = Vb - sqrt( (VT - Vb).^2 + (Vb*delta*T).^2 );

[c,h] = contour(delta,P3,Vds3,[-5:5:20]);
clabel(c,h,'FontSize',14,'LineWidth',1.5);grid on;
set(gca,'FontSize',15);return;

% hold on;
contourf(delta,P3,-Vds3,[0 0],'ShowText','on')
hold on; contourf(delta,P3,Vds3,[-5:5:20],'ShowText','on')
xlabel('\delta');ylabel('P_3 (W)'); set(gca,'FontSize',15);

return;

```

## Appendix(B)

### ZVS DC parameters Code:

```

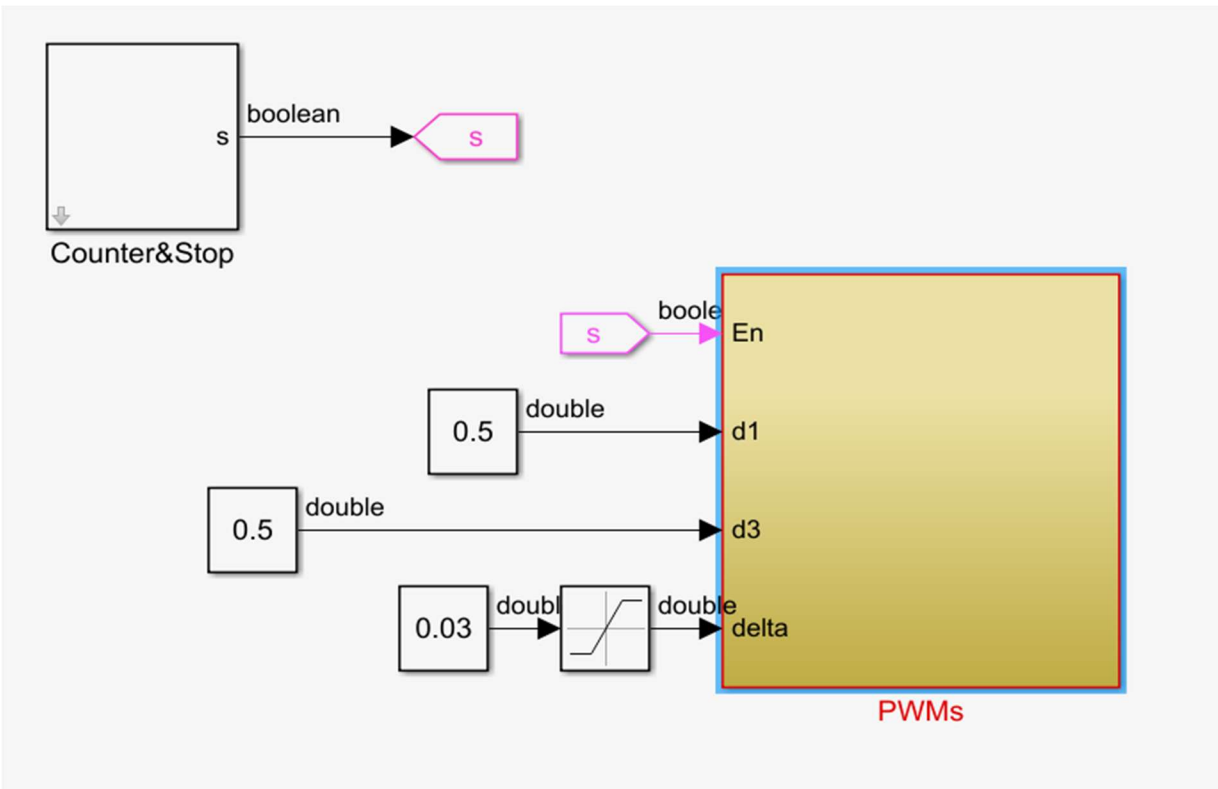
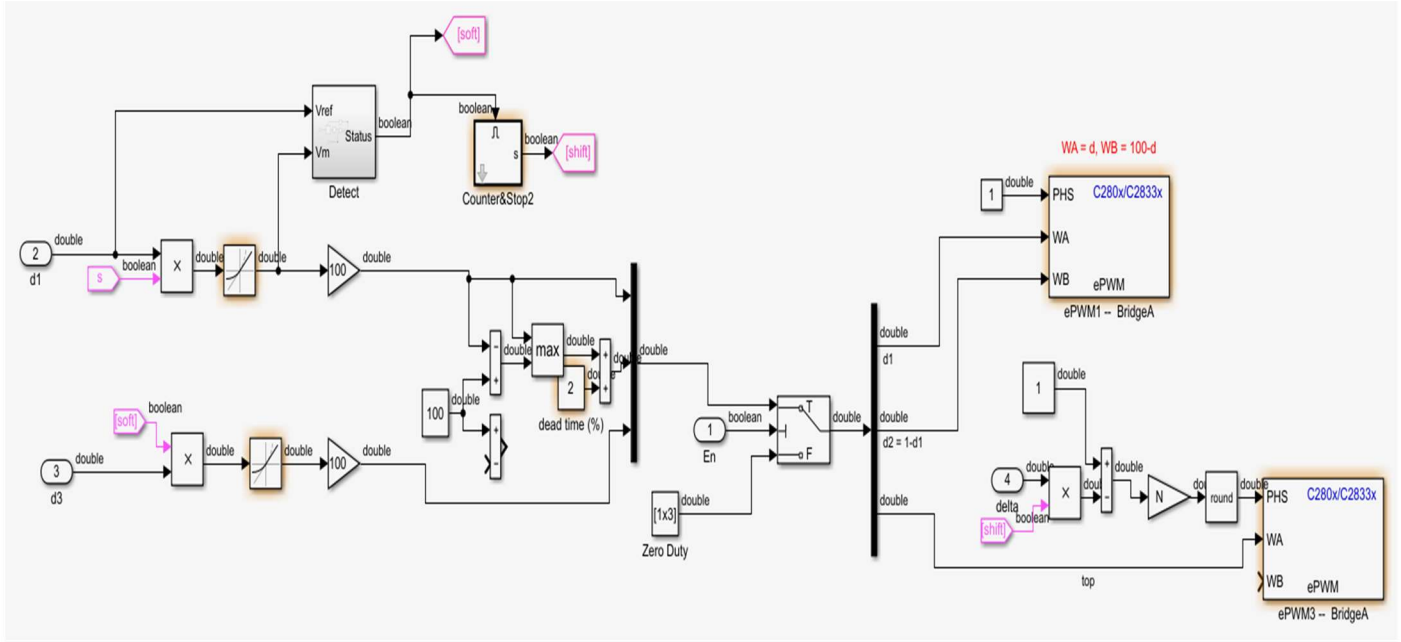
clear all;
Ts = 0.1e-7;
Pn = 120;
T = 10e-6;
tstart = 0.01;
f = 1/T;
n = 50/8;
V1n = 36;
V2n = V1n*n;
R = 300;
Lmg = 85e-6;    % transformer magnetic inductance
Rbase = V1n^2/Pn; Lbase = Rbase/(2*pi*f);
Lm = Lmg/Lbase;
Rm = 1000/Rbase;
Lm = 500; Rm = 500;
% return;
%% PV
Tref = 298; k = 1.38e-23; q = 1.6e-19;
A = 1.2; Eg = 1.11; Vd = 0.55;    % single cell volt
rs = 5e-4;
VT = k*Tref*A/q;
Ks = 0.072; Np = 1;    % Is(T) = Isr*exp(Ks*(T-Tref));
K1 = 3e-3;    % 3mA/degree
Voc1 = 41.6; Isc1 = 5.3;    % BP-175W
% Voc2 = 22; Isc2 = 6.3;    % SW-110W
% Voc1 = 22; Isc1 = 6.3;    % SW-110W
Isr1 = Isc1/exp( Vd/VT );    % saturate @ Tref
Ns1 = floor(Voc1/Vd);
% Isr2 = Isc2/exp( Vd/VT );    % saturate @ Tref
% Ns2 = floor(Voc2/Vd);
Voc = 41.6; Isc = 5.3;    % BP-175W
% Voc = 41.6; Isc = 5.3;    % BP-175W
% lam = 0.7; temp = 298;
% Pm1 = MPPT_Cal(Voc,Isc,lam,temp)
return;
lam = 0.7; temp = 298;
PV2 = MPPT_Cal(Voc1,Isc1,lam,temp); grid on;
max(PV2)

d3 = [0.2 0.3 0.4 0.45 0.5 0.525 0.55 0.6]'-0.03;
Vo = [142 175 193 198 211 223 240 292]';
Vo1 = 2*n*V1n*d3;
[Vo,Vo1]
plot(d3,Vo,'bo-',d3,Vo1,'r-')

```

# Appendix (C)

## Experimental code (Java signal)



## Appendix (D)

### ZVS DC Simulation Controller

